Investigation of Point Doppler Velocimetry (PDV) for Transition Detection in Boundary Layers

John Kuhlman, PI
West Virginia University
Mechanical and Aerospace Engineering Department
Morgantown, WV 26506-6106

Abstract

A two-component Point Doppler Velocimeter (PDV) system has been improved through the use of vapor-limited iodine cells that have responses that are insensitive to temperature variations. Two-component PDV velocity measurements have been obtained for a 1 inch diameter uniform circular jet flow at a nominal exit velocity of 60 m/sec, corresponding to a Reynolds number of 100,000. Similar data have also been obtained for an annular jet and a swirling jet. These PDV data runs have been duplicated to judge the repeatability of these measurements, and also have been compared with hot wire anemometer data for the same flow conditions. PDV mean velocity results are repeatable to within approximately 1-2 m/sec; the PDV RMS velocity results are also quite repeatable. Exit profiles of PDV mean axial velocity data generally agree with hot wire anemometer results to within about 2 m/sec as well. However, the PDV RMS velocity results are consistently lower than the hot wire results everywhere but at the exit of the standard jet, where they are too high relative to the hot wire data. This is believed to at least be partially due to the method used to compute the RMS.

Introduction

Several different non-intrusive whole field velocimetry techniques are currently under development that provide velocity data in a plane, which can thus reduce the time required to map out a complex flow field. This project is exploring the accuracy of Doppler Global Velocimetry (DGV), a nonintrusive, planar imaging, Doppler-based velocimetry technique, as well as the accuracy of related Point Doppler Velocimetry (PDV). Both of these techniques use an iodine vapor cell to determine the Doppler shift, and hence the velocity, of small seed particles in a flow field, as these particles scatter single-frequency laser light that illuminates the flow. The feasibility of the DGV technique for velocity measurement was first demonstrated by Komine of the Northrop Corporation (Komine, et al., 1991). Both DGV and PDV use a heated, temperature-controlled glass cell filled with molecular iodine vapor to measure the Doppler shift of laser light which is scattered off of small, micron-sized seed particles in an air flow. Different velocity components can be measured by viewing the flow from different viewing directions, so that the three-dimensional velocity field can be reconstructed by viewing from three different directions. Molecular iodine vapor exhibits several absorption lines that overlap the green (514.5 nm) wavelength of an Argon ion laser. Other absorption lines overlap the 532 nm wavelength of a pulsed Nd:YAG laser. For DGV, the laser beam is spread into a two-dimensional laser light sheet that illuminates a planar region of the flow of interest. This region is then viewed through the iodine cell by a video camera (in DGV) or photodetector (in PDV) that is used to record the data. The amount of light transmitted through the cell varies as the frequency of the scattered light changes. Regions of different velocity result in different Doppler frequency shifts for this scattered light, which result in different intensities of the light transmitted through the cell and recorded by the detector. To compensate for variations in light intensity across the field of view and variations in the amount of seeding material, the

same region is viewed by a second detector that does not image through the iodine cell, so that the ratio of signal-to-reference detector signals is proportional to the Doppler frequency shift and velocity at a point in the flow.

DGV velocity-measuring technology has several advantages over existing sensors. First, it does not significantly alter the flow patterns being measured, as do pitot or hot wire probes. This is especially critical for recirculating or separated flows. Second, since velocity data are obtained in a planar imaging region, DGV data can be acquired in less time than is required for scanning a point measurement technique such as pitot or hot wire probes, or conventional Laser Velocimetry (LV). This greatly reduces the cost of obtaining such measurements, especially in large wind tunnels. Also, DGV will enable the development of greater insight into the physical behavior of complex flows, which should allow better design and optimization of aerodynamic shapes. Third, DGV is not limited to the measurement of the velocity components in the plane of the laser illumination, as is particle image velocimetry (PIV). Finally, DGV also usually offers the best available spatial resolution, especially in large scale flow facilities. PDV technology is a related technique, where the video cameras are replaced by photodiodes, along with a pair of front lenses and a pinhole, to collect scattered light from a single point in a flow. Once fully developed, PDV may be an attractive alternative to LV, since it is both nonintrusive, as well as being capable of the continuous signal and high data rates typical of hot wire anemometry. This allows the use of well-developed signal processing algorithms for equally-spaced time series data for the calculation of spectra and correlation coefficients.

The WVU DGV research group has been concentrating on carefully documenting the achievable accuracy for typical DGV and PDV systems. Dominant error sources are being determined, and system improvements are being developed to increase accuracy. This is being done by measuring the velocity fields in simple, known flows such as fully developed turbulent pipe flow, jet flows, and a turbulent flow over an airfoil. Also, a simple rotating disk has been used as a velocity standard. Results obtained for the rotating disk using the WVU PDV system gave accuracies of total measurement range on the order of 1-2% of full scale (0.5-1 m/sec) over a velocity range of approximately 60 m/sec. Results for the WVU DGV system were accurate to between 3-6% of full scale (1.5-3 m/sec) over the same velocity range. However, a time-varying mean velocity offset error was observed for all of these earlier DGV and PDV results that was as large as 8 m/sec, but usually between 2-5 m/sec. It was found that the major cause of this error was the randomly varying stem temperatures of the iodine cells used for these measurements (Naylor and Kuhlman, 2000). Since these early cells contained both solid and vapor iodine, a stem temperature variation with an RMS of as little as $\pm 0.1^{\circ}C$ would result in the observed velocity offset error, by changing the cell response. These results may be viewed in a series of papers at http://www.cemr.wvu.edu/~jkuhlman/DGV.html, and a Ph.D. dissertation by Naylor (1998) at http://157.182.199.25/etd/ETDS/E116/. The WVU DGV and PDV work has been cited in a recent survey of the state of the art in DGV capability by Elliott and Beutner (1999).

The goals of the present work are: 1.) to study the accuracy of the PDV instrument fitted with new vapor-limited iodine cells that should greatly reduce the earlier mean velocity offset error, 2.) to study the utility and accuracy of the PDV system for the measurement of turbulent flow,

and 3.) to study the utility of the PDV system for the detection of transition from laminar to turbulent flow. A related study of the applicability of PDV to turbulent flow measurements for the flow over a NACA 0012 airfoil has been described in Webb, 1999 and Kuhlman and Webb, 1999, although these data were obtained before the vapor-limited iodine cells were received.

Apparatus and Procedure

The present PDV system has been patterned after the basic DGV technology originally developed by Meyers, et al. (1991), in an effort to document the accuracy that is attainable with such systems. The original PDV system hardware and software have been described in more detail in Kuhlman, et al. (1997), and in the theses by James (1997) and Webb (1999). An iodine cell has been used to monitor laser frequency drift. This laser frequency monitoring system is shown in Fig. 1. The present vapor-limited iodine cells (Fig. 2) are 3" in diameter, with a 5" optical path length, and contain only vapor phase iodine when operated at or above their filling temperature of 43 °C, and have been supplied by Innovative Scientific Systems, Inc. (ISSI), of Dayton, OH. Cell design has been patterned after the vapor-limited iodine cells used by Elliott (Elliott, et al., 1994; Mosedale, et al., 1998). For the present work, these cells have been operated at a body temperature of 80 °C. Long term drift in iodine cell stem temperature has been measured to be on the order of ± 0.1-0.2 °C, once the cells have warmed up to the steady operating temperature of 80 °C, and short-term stem temperature fluctuations have an RMS of 0.1 °C or less. Neutral density filters and a beam expander are used to ensure that neither the iodine cell nor either photodiode of the laser frequency monitoring system is saturated by the reference beam. The laser used is a Coherent Innova 305 argon ion laser fitted with an etalon for single mode operation, delivering approximately 1W of single frequency light at 514.5 nm. A laser spectrum analyzer has been used to monitor laser mode shape and to detect the occurrence of mode hops.

Data acquisition and data reduction software has been developed in Visual Basic 4.0; see James, 1997, Naylor, 1998, and Webb, 1999 for details. An 8 channel, 16 bit, simultaneous-sample-and-hold IOTech model ADC488-16 A/D board is used for digital data acquisition of the photodetector output voltages for the frequency monitoring system and the two PDV components. The RMS noise level for this board is ± 0.3 mV on a 10 volt scale.

A rotating wheel apparatus has been previously used to determine the accuracy of the two-component PDV system. This wheel has a maximum linear velocity of approximately ± 29 m/s. A fully developed turbulent pipe flow apparatus has been developed, using 1.5 inch diameter pipe with a length-to-diameter ratio of 60 (Naylor, 1998). For the present work, a 1" diameter uniform axisymmetric jet flow facility has also been developed. A jet has been chosen for the present study because it is a well-documented simple turbulent flow (Wygnanski and Fiedler, 1969; Kuhlman and Gross, 1993) with important technological applications, that can easily be made more complex through addition of either swirl or non-uniform exit mean velocity profile shape (annular jet; Kuhlman, 1987). Kuhlman (1994) has reported conventional LV data for the standard uniform exit velocity jet and the annular jet. Hussain, et al. (1988) have compared LV and hot wire data in a standard jet, and found significant errors in hot wire data at the edges of such a jet flow.

The jet is fed from a plenum fitted with a flow-straightening element, via a 16:1 area ratio nozzle. This nozzle has been fitted with an annular centerbody to create the annular jet with a

low axial velocity on the centerline at the exit (Kuhlman, 1987), or with a swirler to create a swirling jet having an exit swirl number of approximately 0.33. The flow is driven by a variable-speed blower, which can achieve exit velocities of just over 100 m/sec. For the present results, the jet has been run at an exit velocity of nominally 60 m/s, corresponding to a Reynolds number of 100,000. Flow seeding for PDV measurements is provided by a commercial ROSCO fog machine, which feeds a large plenum, to damp out pulsations in smoke output. This has led to improved uniformity in the signal levels over time for the present jet flow data. Also, the amount of smoke produced has been reduced by placing a diode in series with the motor that drives the fog fluid pump. This has improved the quality of data, most likely by allowing data to be taken at lower seeding levels, thus reducing the effects of secondary scattering.

A computer-controlled, three-axis traversing system has been developed, as described in the thesis by Ramanath (1997), for use in positioning the flow facilities with respect to the fixed PDV system, so that velocity contours may be mapped out in a series of traverses across the jet flow (radial direction), or along the jet axis (axial direction). Accuracy of a single traverse move has been found to be on the order of 0.001" for typical moves on the order of a few inches.

Fig. 3 shows one of two PDV channels. Photodiodes, along with front lenses and pinholes, are used to collect scattered light from a single point in a seeded flow. Kuhlman, et al. (1997) and James (1997) have described the original PDV system in detail. For the present work, the original photodetectors have been replace by Thor Labs PDA55 photodiodes, which have 5 different selectable, fixed amplifier gains. These photodiodes have less noise and less DC offset than those used previously. Also, the original beamsplitters have been replaced by custom Melles Griot "polarization-insensitive" beamsplitters (specified as uniform versus polarization axis to ±3% at 45°). Polarizing filters have been placed in front of the beam splitters to minimize effects due to any residual polarization sensitivity of the beam splitters. Calibration of the 3 iodine cells has been accomplished in situ, with the cells installed ready for data acquisition, using a continuous scan of the mode structure of the cw Argon ion laser by mechanically altering the tilt of the etalon through about 10-20 mode hops (James, 1997). Light is scattered off of the same smoke particles as are used in the actual jet flow, but at a much lower air velocity (~1-2 m/sec).

Radial and axial jet mean and RMS velocity profiles have been obtained by traversing the jet flow facility slowly with respect to the fixed PDV systems using the traverse (at a rate of 0.1"/sec), while continuously recording the photodiode voltages using the A/D system. For the present data a sampling rate of 100 Hz has been used, although significantly higher rates are possible. These "strip chart" data records have been repeated 10 times for each radial or axial profile. Average velocity results have then been obtained by smoothing the individual time records by computing 10-point running average and RMS values, and then averaging these smoothed signals for the 10 separate traverses. Thus, each average and RMS data point presented is effectively based upon a 1 second time average, at a sampling rate of 100 Hz. During the 0.1 second over which the smoothing operation is performed, the traverse moved the jet flow a distance of 0.01", which is relatively small compared to the nominal 2 mm

diameter of the sampling volume for the PDV system. PDV photodiode voltage signals are on the order of 1V for the forward scatter and 0.1V for the backscatter photodetectors. 2-component PDV data has been obtained for the uniform exit velocity standard jet, the swirling jet, and the annular jet for centerline traverses and radial traverses at x/D = 0.25, 1, 2, (3), 4, 6, 8, 10, and 12. For each jet configuration, additional runs have been made to assess data repeatability. Also, single-component constant temperature hot wire anemometer data has been acquired for the standard jet and the swirling jet, for comparison with the PDV results.

Results

Early PDV data repeatability, as documented in the thesis by Ramanath (1997), was poor. However, improved cell calibration procedures (James, 1997) significantly increased PDV and DGV system accuracy. Both single and 2-component PDV data measured on a rotating wheel have been presented by James (1997), and by Kuhlman, et al. (1997). Total wheel velocity range was 57 m/sec, so the observed the velocity range error magnitudes of approximately ±0.6-1.2 m/sec, correspond to 1-2 % errors. Also, the standard deviations of the actual PDV wheel velocity data points from the least squares linear curve fits was 0.5-0.7 % (0.3-0.5 m/sec). This RMS error is approximately 2-3 times smaller than has been documented by other DGV or PDV researchers. Two-component PDV data obtained from a traverse across the exit of the fully developed pipe flow at a nominal Reynolds number of 76,000, have been previously presented by Kuhlman (1998). The axial mean velocities agreed well with results from a pitot-static probe survey. Turbulent velocity levels generally agreed with hot wire data of Laufer (1954).

However, all of these earlier results exhibited a slow, long-term drift in the recorded value of zero mean velocity. This mean velocity "offset error" was typically on the order of 2-6 m/sec, and appeared to vary randomly with time. It has been found that this offset error was largely due to the random, uncorrelated variations in iodine cell stem temperatures (Naylor and Kuhlman, 2000). This stem temperature variation has been observed to vary with a short term RMS of 0.1 degrees C (Naylor, 1998). For the original iodine cells used in the DGV and PDV systems, increasing the cell stem temperature would increase the amount of vapor phase iodine in the body of the cell, thus altering the cell absorption. This has been found to correspond to an error in the computed Doppler shift frequency of 7 MHz, using the iodine absorption model of Forkey (Forkey, et al., 1995). This then corresponds to a mean velocity error of from 2 to 10 m/sec, depending on the geometry and viewing direction of the PDV system (Naylor and Kuhlman, 2000). This level of velocity error is consistent with the observed mean velocity offset error for this early work.

Configuration geometry for the present jet flow measurements is shown in Fig. 4. A large cone has been connected to a blower to exhaust the seeded flow from the laboratory. One PDV component has been configured in forward scatter, and is primarily sensitive to the jet axial velocity, while the other PDV channel has been operated in backscatter and primarily senses the jet circumferential velocity. However, as a result, the backscatter channel signal strength is only about 10 % as large as the forward scatter signal. The speed of the blower that feeds the pipe flow apparatus has been adjusted to balance the jet flow rate and entrainment with the maximum exhaust blower flow rate. This yielded a nominal centerline exit velocity of 60 m/sec based on pitot-static probe data, corresponding to an exit Reynolds number of 100,000 based on the jet exit diameter.

Examples of the 2-component PDV velocity data in the uniform circular jet are presented in Figs. 5-13. Data have been obtained for lateral traverses at x/D = 0.25, 1, 2, 4, 6, 8, 10, and 12, where both the measured mean and RMS axial and circumferential velocities are shown. Fig. 13 presents the corresponding centerline profiles of mean and RMS velocities. Mean axial velocity profiles (Figs. 5-12) appear to become self-similar beyond about x/D = 6. Centerline mean axial velocity (Fig. 13) shows a slight decay (approximately 5 m/sec) over the first 3 jet diameters, as has been seen in the DGV data of Thorpe, et al. (1996). However, pitot-static and hot wire measurements in this flow do not exhibit this drop in centerline velocity, instead indicating a potential core extending 4-5 diameters from the exit. Longmire and Eaton (1990) also do not see a similar decay in their study of a lightly-loaded particle-laden circular air jet. The cause of this centerline mean axial velocity decay near the jet exit for the PDV results is at present unknown. Mean circumferential velocities, which should everywhere be equal to zero in this flow, display an offset that varies from 1 m/sec near the jet exit, to a maximum value of between 2 and 2.5 m/sec at large x/D. This variation is speculated to be the result of inaccuracies in the iodine cell calibration curves which might be larger at different ratio values. The present PDV data has been obtained for a ratio range for the laser frequency monitoring system of nominally 0.4-0.6, with the ratio value outside of the absorption line of 0.89. Exit RMS velocities are on the order of 1.0-1.5 m/sec; it is possible that this may actually be indicative of the lowest sensitivity of the current PDV system to velocity fluctuations. This minimum measured turbulence intensity of about 1.7% approaches the sensitivity to turbulence typically achievable with conventional counter-processor-based LV systems. Centerline RMS velocities (Fig. 13) increase from their exit levels of about 1 m/sec to maximum values (of about 5.5 m/sec-axial; 4.5 m/sec-circumferential) at about x/D = 6, and then slowly decay. The axial and circumferential RMS velocities for traverses at x/D = 6 and beyond are nearly equal, with the axial RMS slightly higher, as would be expected in a circular jet flow (Wygnanski and Fiedler, 1969). Also, the centerline axial turbulence intensity at x/D = 12 is about 19 %, in agreement with previous measurements (Kuhlman, 1994). Wyganaski and Fiedler found a centerline axial turbulence intensity of 28% in the far-field self-preserving region of their jet flow (beyond about 50-70 jet diameters), indicating that the present data are still in the near-field region.

Mean velocities exhibit a variability from a smooth curve in any one traverse profile of less than 1 m/sec at the exit (Fig. 5) to as much as 2-3 m/sec at large x/D (Figs. 10-13). Variability of the corresponding computed RMS velocity profiles varies from less than 0.5 m/sec at the exit to as much as 1.5 m/sec at x/D = 12. This decrease in the smoothness of the profiles as x/D increases is due to the increased turbulence time scale farther from the jet exit. This variability in the results is not due to any limitation in the PDV system itself, and could be significantly reduced by increasing the averaging time for data at large x/D values. It has been observed that the present PDV data do not exhibit any of the drift in the zero velocity offset that had been observed with the previous iodine cells. It now appears that a dominant error source is the accuracy of the iodine cell calibrations, estimated as on the order of about ±1-2 m/sec. Similar data sets are presented below for the annular jet, as well as for the swirling jet at an exit swirl number of approximately 0.33, where the circumferential mean velocity is non-zero. Both of these configurations exhibit increased turbulence levels and mixing compared to the uniform jet, and have similar levels of mean velocity offset (always no more than 2-3 m/sec, on the same order as the estimated current calibration accuracy).

Figs. 14 and 15 present the axial mean and RMS velocity data presented above in Figs. 5-12, but with all profiles shown versus r/D on single graphs. This helps to summarize the general behavior of the standard jet at a glance. Similar data are shown in Figs. 16 and 17 for a repeat run of the standard jet, performed on a different day with different iodine cell calibrations, to assess the repeatability of the PDV data. These data generally match those of the first run to within about ±1-2 m/sec.

Similar summary plots of the axial mean and RMS velocities for the annular jet are shown in Figs. 18-21 for two runs performed on the same day, using two different iodine cell calibrations. Again, repeatability for these two runs is observed to be about ±1 m/sec. This annular jet has an exit mean axial velocity profile that displays a low velocity central core (about 25 m/sec on the centerline, versus a maximum of 56 m/sec; see Figs 18 and 20), so that in effect the annular jet possesses both an outer jet shear layer as well as an inner "wake" type of shear layer. This leads to increased turbulence levels relative to the standard uniform jet, as well as enhanced mixing, and faster centerline velocity decay. Thus, the mean axial velocity at x/D = 12 is only about 10-12 m/sec for this annular jet (Figs. 18 and 20), as compared to a value of about 28-30 m/sec (Fig. 13) for the standard jet. The mean axial velocity profiles at the exit are not axisymmetric; instead the high velocity peaks differ on opposite sides of the jet. This has been found to be due to a slight asymmetry in the mounting of the cylindrical centerbody in the nozzle. This centerbody creates the low velocity central core. This asymmetry is gone by x/D = 2, and the mean axial velocity profiles appear to become self-similar by x/D = 3. Offset in the circumferential mean velocity from the expected value of zero ranges from 0-2 m/sec for these two runs; this is consistent with the ranges seen for the standard jet. Also, variability of the radial profiles of mean velocity from smooth curves again ranges from 0.5-1 m/sec near the exit to 2-3 m/sec at x/D = 12. RMS velocity profiles show a variability from smooth curves of about 1 m/sec for all x/D. The measured RMS velocity data result in calculated turbulence intensities of between 10-15% near the exit to 25-28% at x/D = 12. Similar behavior in the annular jet was observed for a series of single-component conventional LV data by Kuhlman (1994).

Examples of the 2-component PDV velocity data in the swirling jet are presented in Figs. 22-30. Data have been obtained for lateral traverses at x/D = 0.25,1,2,3,4,6,8,10, and 12, where again both the measured mean and RMS axial and circumferential velocities have been shown. Fig. 31 presents the corresponding centerline profiles of mean and RMS velocities. Exit mean axial velocity profile is nearly uniform (Fig. 22), similar to the standard jet case (Fig. 5), but with a thicker outer shear layer. Mean axial velocity profiles (Figs. 22-30) again appear to become self-similar beyond x/D = 6. Centerline mean axial velocity (Fig. 31) begins to decay immediately beyond the exit, with no evidence of a potential core. As a result, even though both the uniform and swirling jets both have exit velocities of about 58-60 m/sec, the mean axial velocity of the swirling jet has decayed to about 20 m/sec at x/D = 12, compared to a value of about 28-30 m/sec for the uniform jet (Fig. 13). Mean swirl velocity profile at the exit (Fig. 22) is antisymmetric, and displays a near-rigid body rotation profile near the centerline ($r/D \leq 0.2$), but then levels off to a nearly constant swirl mean velocity of ±20 m/sec until $r/D \cong 0.4$. This results in an exit swirl number for this jet of nominally 0.33, based upon the maximum swirl and axial velocities at the exit. The maximum swirl velocity for a radial profile decays rapidly along the jet axis, having decayed to a maximum of ±10 m/sec at x/D = 3 (Fig.

25), ±5 m/sec at x/D = 6 (Fig. 27), and ±1-2 m/sec at x/D = 10 and 12 (Figs. 29-30). Beyond x/D = 6 the measured mean swirl velocity profiles are essentially a solid body rotation for the entire radial direction measurement range. These mean circumferential velocity measurements again display offsets of between 1 m/sec at the exit to maximum values of approximately 2 m/sec for large x/D. Exit RMS velocity levels (Fig. 22) are higher than for the standard uniform jet (Fig. 5), and exit axial RMS is less than swirl RMS (about 1 m/sec, versus 2 m/sec). Both RMS velocities increase versus x/D (Fig. 31), reaching peak values at about x/D = 3, and then decay slowly. Note that the swirl RMS velocities are larger than the axial RMS velocities until about x/D = 8-10; beyond this both RMS velocities appear to be approximately equal. At x/D = 12 the turbulence centerline intensities are about 25-28%. Thus, it is noted that $x/D \geq 8$ is the region where the mean axial velocity profiles appear to be self-similar, the mean swirl velocity profiles appear as a solid body rotation, and the axial and swirl RMS velocities appear to be nearly equal. The observed levels of variability of the mean and RMS data for the radial profiles (Figs. 22-30) are quite similar to those observed for the standard jet (Figs. 5-12). The increase from less than 1 m/sec at the exit to 1.5-3 m/sec at large x/D is again due to the increased turbulence time scales as x/D increases. Finally, it is remarked that during the data runs, it was possible to observe the core of the vortex for this swirling jet on the jet axis for $0 \leq x/D \leq 4$.

Composite plots of mean and RMS axial and circumferential velocity results for two swirling jet runs are presented in Figs. 32-39. Comparison of the two runs again shows a repeatability between runs of about 1-3 m/sec. The exit axial mean velocity profiles differ by about 3-3.5 m/sec; it is believed that this may have been due to the installation of new brushes in the blower motor immediately prior to the first of the two swirling jet runs.

Comparisons between PDV and hot wire anemometer axial velocity results are shown in Figs. 40-41 for the standard jet and in Figs. 42-43 for the swirling jet. These hot wire data were taken at a sampling rate of 10 kHz, and data records were 0.8 seconds in length. PDV mean axial velocity results at the jet exit generally agree with the hot wire data to within about 2 m/s for both jets (Figs. 40 and 42). However, the exit profiles of PDV RMS velocities do not agree with the hot wire results. PDV RMS is too high for the standard jet (Fig. 40) and too low for the swirling jet (Fig. 42). Note the unrealistic hot wire RMS on the centerline of the swirling jet; this is likely due to enhanced cooling by the swirl velocity. Agreement between the PDV and hot wire mean axial velocity results for centerline traverses (Figs. 41 and 43) is generally not as good as is observed for the exit profiles. However, it is noted that these mean velocity results agree to within about 2 m/s for x/D between 9 and 12 for the standard jet (Fig. 41) and for x/D between 5 and 12 for the swirling jet. As was observed for the exit profiles, the PDV RMS velocity results do not agree well with the hot wire results.

Conclusions

A two-component Point Doppler Velocimeter (PDV) system has been significantly improved in the present work through the use of vapor-limited iodine cells that are not sensitive to temperature variations. Two-component PDV velocity measurements have been obtained for a 1 inch diameter uniform circular jet flow at a nominal exit velocity of 60 m/sec, and similar results have also been obtained for an annular jet and a swirling jet. These PDV data runs have been duplicated to judge the repeatability of these measurements, and also have been compared

with hot wire anemometer data for the same flow conditions. PDV mean velocity results are repeatable to within approximately 1-2 m/sec; the PDV RMS velocity results are also quite repeatable. Exit profiles of PDV mean axial velocity data generally agree with hot wire anemometer results to within about 2 m/sec as well. However, the PDV RMS velocity results are consistently lower than the hot wire results everywhere but at the exit of the standard jet, where they are too high relative to the hot wire data. This is believed to at least be partially due to the method used to compute the RMS. It is recommended that PDV data be acquired in the same fashion as that used for the hot wire results to confirm this hypothesis.

Acknowledgements

The present work has been supported under NASA Langley Research Center Grants NAG-1-1892 and NAG-1-2132, Mr. James F. Meyers, technical monitor. Additional support under AFOSR/DEPSCoR Grants F49620-94-1-0434 and F49620-98-1-0068, Drs. J. M. McMichael, M. Glauser, and T. Beutner, technical monitors, is also acknowledged.

References

Elliott, G. S., Samimy, M., and Arnette, S. A., "Details of a Molecular Filter-Based Velocimetry Technique," paper AIAA - 94-0490, AIAA 32nd Aerospace Sciences Meeting, Jan. 10-13, 1994, Reno, NV.

Elliott, G. S. and Beutner, T. J., "A Review of Recent Advancements in Molecular Filter Based Planar Doppler Velocimetry Systems," Progress in Aerospace Sciences, Vol. 35, 1999, pp.799-845.

Forkey, J.N., Finklestein, N.D., Lempert, W.R., and Miles, R. B., "Control of Experimental Uncertainties in Filtered Rayleigh Scattering Measurements," paper AIAA-95-0298, presented at AIAA 33rd Aerospace Sciences Meeting, Jan. 9-12, 1995, Reno, NV; also AIAA Journal, Vol. 34, No.3, Mar. 1996, pp. 442-448.

Hussain, H. J., George, W. K., and Capp, S. P., "Comparison between Hot-Wire and Burst-Mode LDA Velocity Measurements in a Fully-Developed Turbulent Jet," paper AIAA-88-0424, presented at AIAA 26th Aerospace Sciences Meeting, Jan. 11-14, 1988, Reno, NV.

James, K., "Determination of the Accuracy of a Two-Component Point Doppler Velocimetry System," MS Thesis, West Virginia University, MAE Department, 1997.

Komine, H., Brosnan, S. J., Litton, A. B., and Stappaerts, E. A, "Real-Time Doppler Global Velocimetry," paper AIAA-91-0337, AIAA 29th Aerospace Sciences Meeting, Jan. 7-10, 1991, Reno, NV.

Kuhlman, J. M., "Variation of Entrainment in Annular Jets," AIAA Journal, Vol. 25, No. 3, March 1987, pp. 373-379.

Kuhlman, J. M. and Gross, R. W., "Three-Component Velocity Measurements in an Axisymmetric Jet using LDV," DANTEC Information, No. 12, Feb. 1993, pp. 10-16.

Kuhlman, J. M., "Turbulence Measurements in Annular Jets Using Laser Velocimetry," presented at ASME Symposium on Laser Anemometry: Advances and Applications, Lake Tahoe, NV, June 19-23, 1994.

Kuhlman, J. M., Naylor, S., James, K., and Ramanath, S., "Accuracy Study of a 2 – Component Point Doppler Velocimeter (PDV)," paper AIAA-97-1916, presented at AIAA 28th Fluid Dynamics Conference, Snowmass, CO, June 29-July 2, 1997.

Kuhlman, J., "Development of Doppler Global Velocimeter," Final Report for AFOSR/DEPSCoR Grant F49620-94-1-0434, May, 1998.

Kuhlman, J. M. and Webb, D. L., "2-Component Point Doppler Velocimetry (PDV) Measurements of Turbulent Flow over an Airfoil," paper AAIAA-99-3517, presented at AIAA 30th Fluid Dynamics Conference, June 28-July 1, 1999, Norfolk, VA.

Laufer, J., "The Structure of Turbulence in Fully Developed Pipe Flow," NACA TR 1174, 1954.

Longmire, E. K. and Eaton, J. K., "Structure and Control of a Particle-Laden Jet," Report No. MD-58, Dept. of Mechanical Engineering, Stanford Univ., Stanford, CA, Sept. 1990.

Mosedale, A., Elliott, G. S., Carter, C. D., and Beutner, T. J., "On the Use of Planar Doppler Velocimetry," paper AIAA-98-2809, AIAA 20th Advanced Measurement and Ground Testing Conference, June 15-18, 1998, Albuquerque, NM.

Meyers, J. F., Lee, J. W., and Cavone, A. A., "Signal Processing Schemes for Doppler Global Velocimetry," 14th International Congress on Instrumentation in Aerospace Simulation Facilities, Rockville, MD, Oct. 27-31, 1991.

Meyers, J. F., "Doppler Global Velocimetry, The Next Generation?," paper AIAA-92-3897, presented at AIAA 17th Ground Testing Conference, July 6-8, 1992, Nashville TN.

Meyers, J. F., "Evolution of Doppler Global Velocimetry Data Processing," 8th Int'l. Symp. On Applications of Laser Techniques to Fluid Mechanics, July 8-11, 1996, Lisbon, Portugal.

Naylor, S. and Kuhlman, J., "Accuracy Studies of a Two-Component Doppler Global Velocimeter (DGV)," paper AIAA-98-0508, AIAA 36th Aerospace Sciences Meeting, Jan. 12-15, 1998, Reno, NV.

Naylor, S. and Kuhlman, J., "Results for a Two-Component Doppler Global Velocimeter (DGV)," paper AIAA-99-0268, AIAA 37th Aerospace Sciences Meeting, Jan. 11-14, 1999, Reno, NV.

Naylor, S. and Kuhlman, J., "Results for a Two-Component Doppler Global Velocimeter (DGV)," AIAA Journal, Vol. 38, No. 5, May 2000 (at press).

Naylor, S., "Development and Accuracy Determination of a Two-Component Doppler Global Velocimeter (DGV)," PhD Dissertation, West Virginia University, MAE Department, 1998.

Ramanath, S., "Development of a Point Doppler Global Velocimeter (DGV)," MS Thesis, West Virginia University, MAE Department, 1997.

Thorpe, S. J., Ainsworth, R. W., and Manners, R. J., "Time-Averaged Free-Jet Measurements Using Doppler Global Velocimetry," ASME Fluids Engineering Div. Conf., FED-Vol. 239, Volume 4, 1996.

Webb, D. W., "Development of and Measurements using a Point Doppler Velocimetry (PDV) System,' MS Thesis, West Virginia University, MAE Department, 1999.

Wygnanski, I. and Fiedler, H., "Some Measurements in the Self-Preserving Jet," Journal of Fluid Mechanics, Vol. 38, Part 3, 1969, pp. 577-612.

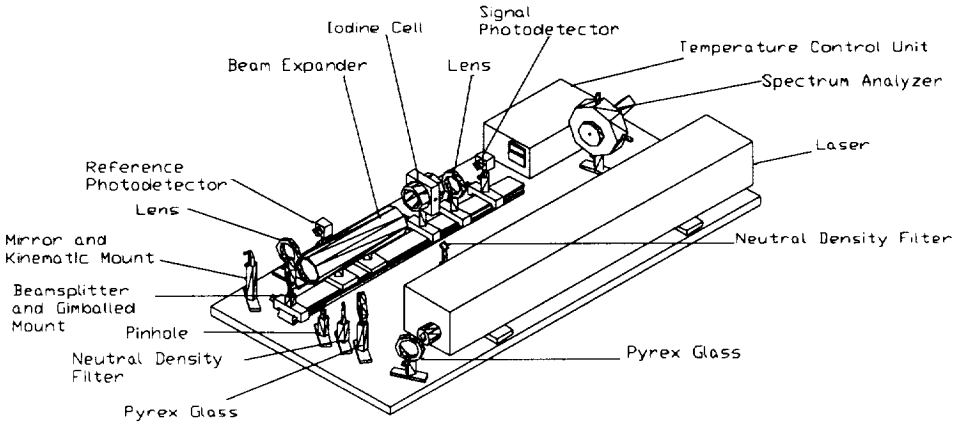

Fig. 1 Schematic of laser frequency monitoring system

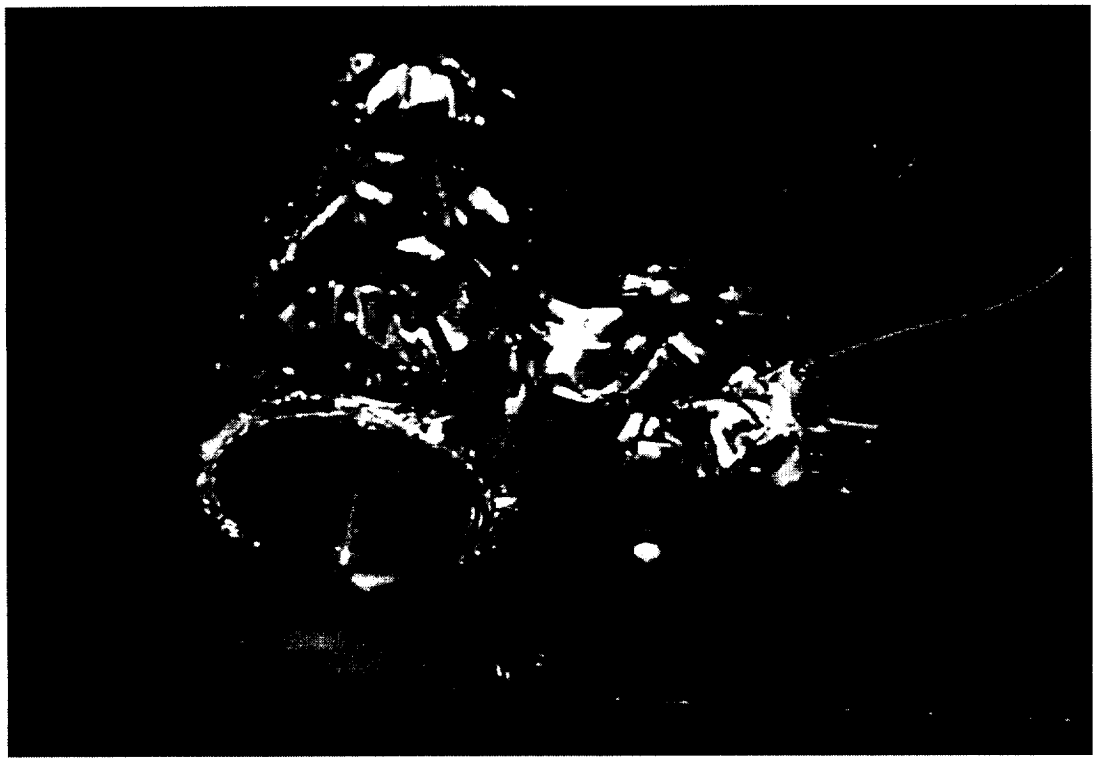

Fig. 2. Iodine cell wrapped in heater tape and metal foil

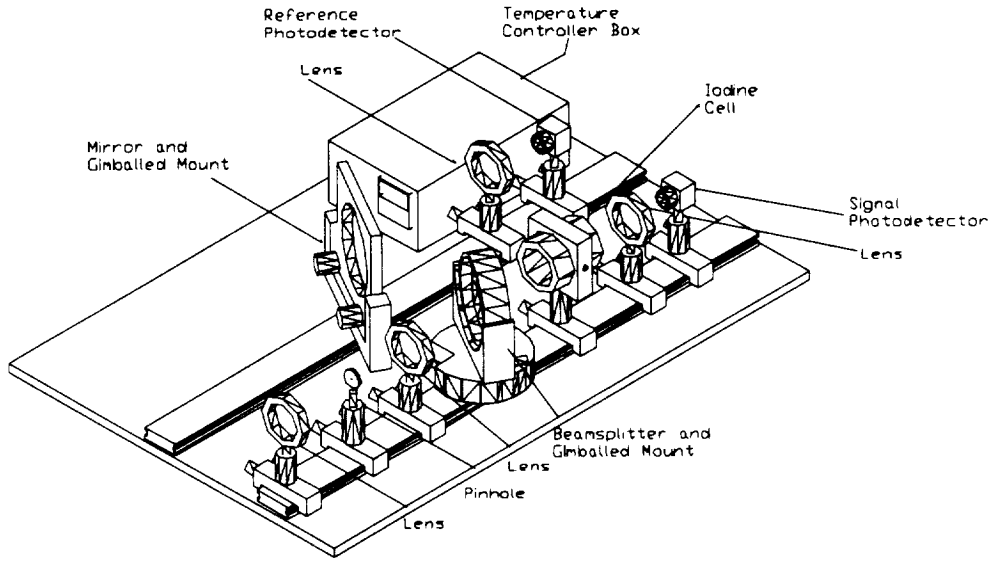

Fig. 3 Schematic of PDV velocity measuring component

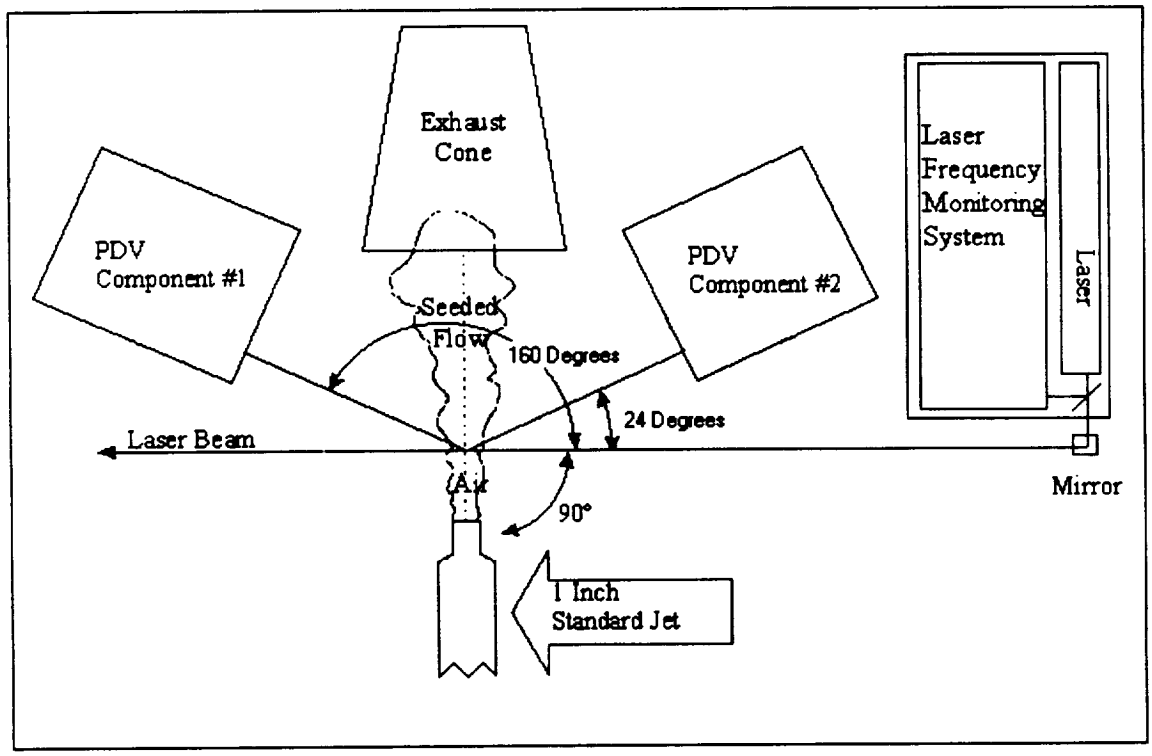

Fig. 4 Overhead Schematic of PDV setup with typical component angles

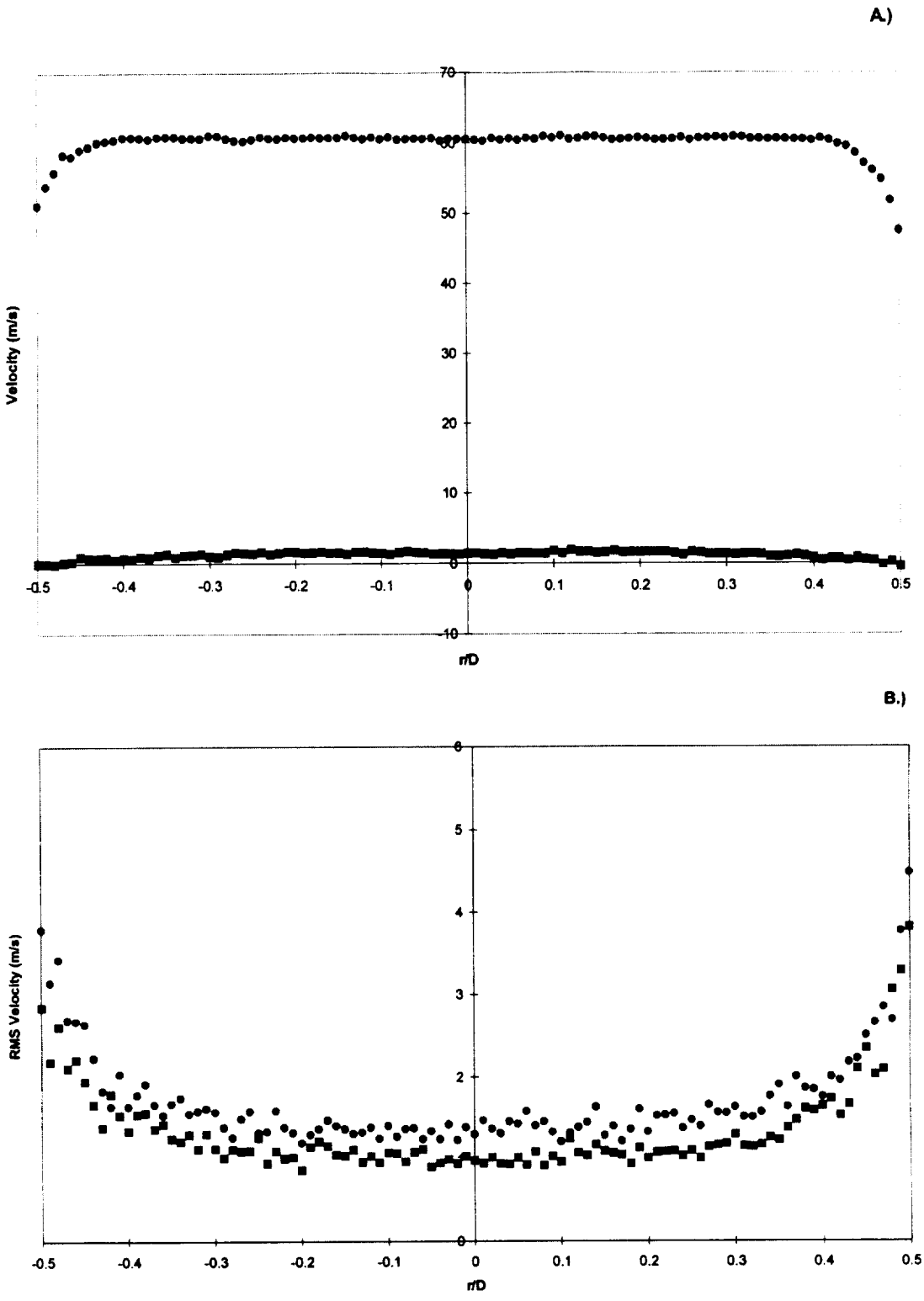

Fig. 5 2-Component PDV velocity results for standard jet; x/D = 0.25;
Circles-axial velocity; Squares-circumferential velocity
a.) mean velocities
b.) RMS velocities

10-1-99

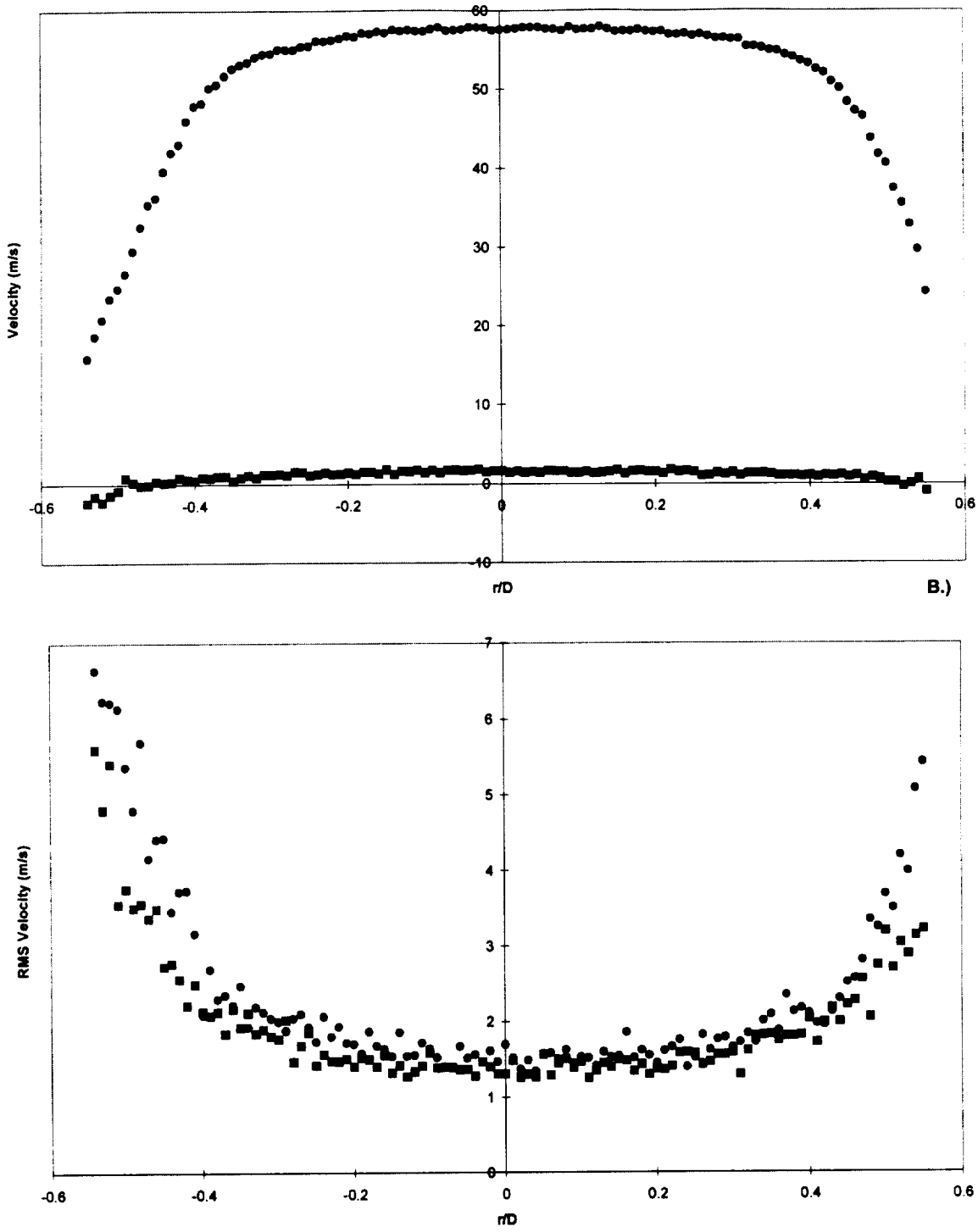

Fig. 6 2-Component PDV velocity results for standard jet; x/D = 1;
Circles-axial velocity; Squares-cicumferential velocity
a.) mean velocities
b.) RMS velocities

10-1-99

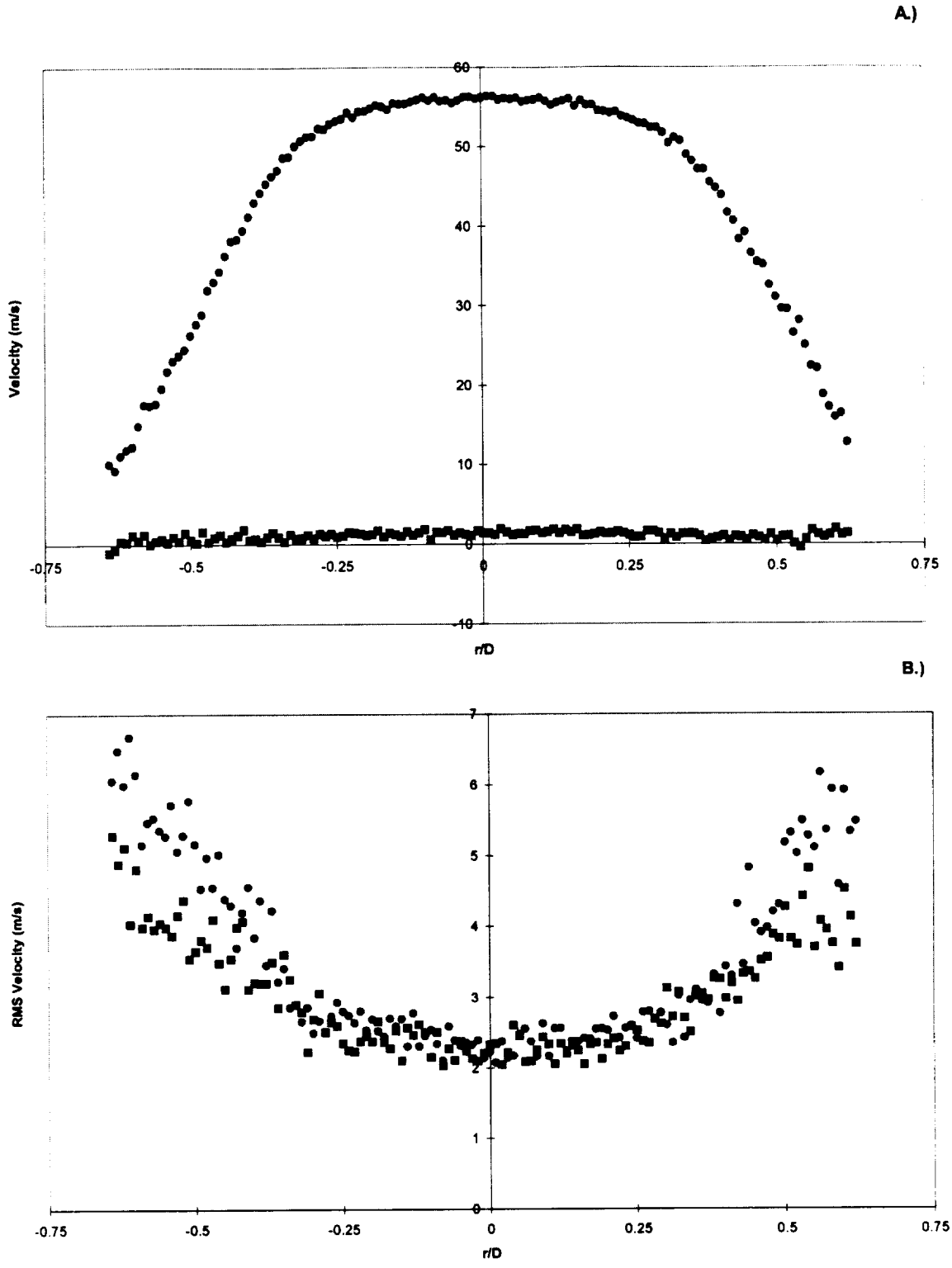

Fig. 7 2-Component PDV velocity results for standard jet; x/D = 2;
Circles-axial velocity; Squares-cicumferential velocity
a.) mean velocities
b.) RMS velocities

10-1-99

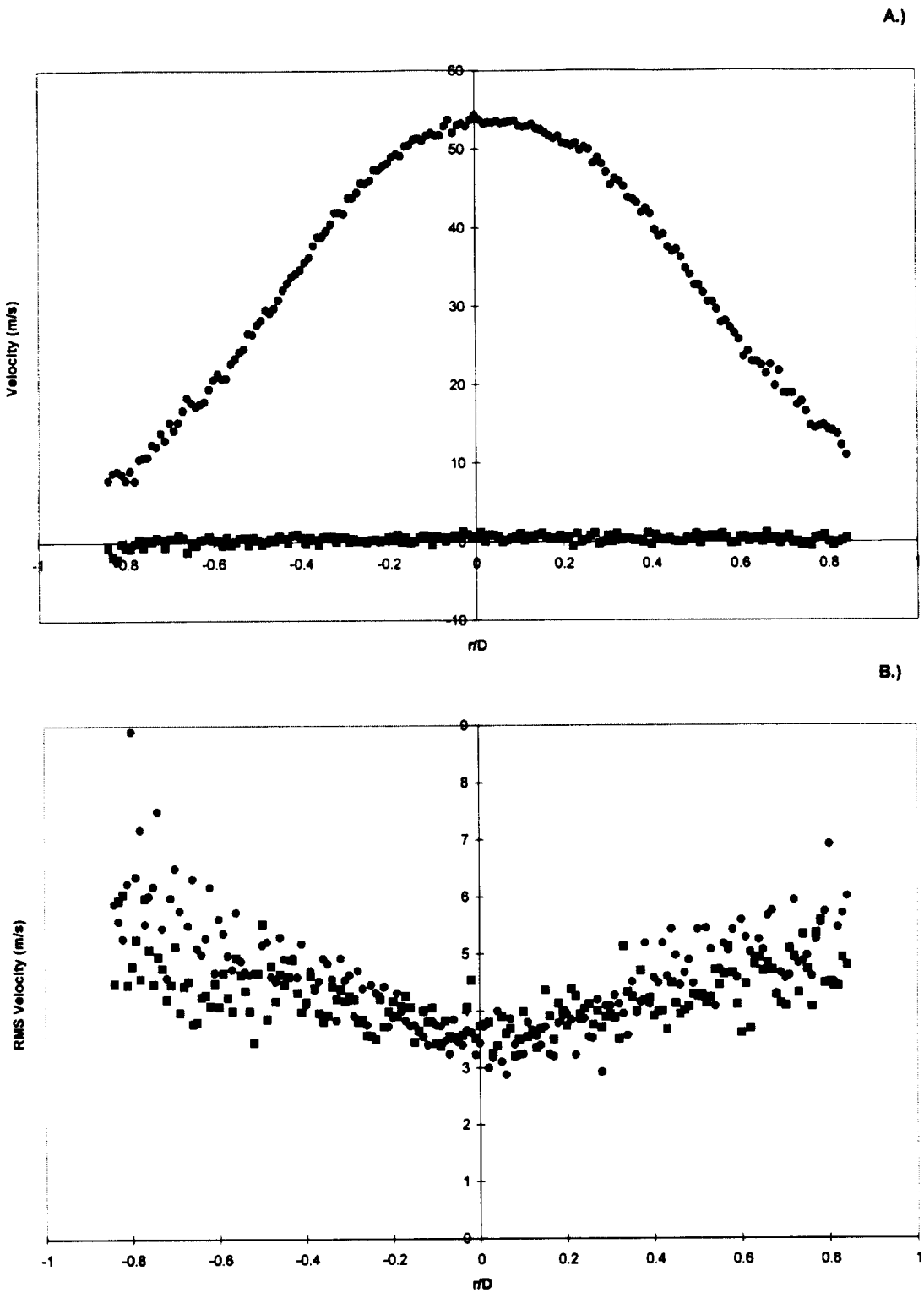

Fig. 8 2-Component PDV velocity results for standard jet; x/D = 4;
Circles-axial velocity; Squares-cicumferential velocity
a.) mean velocities
b.) RMS velocities

10-1-99

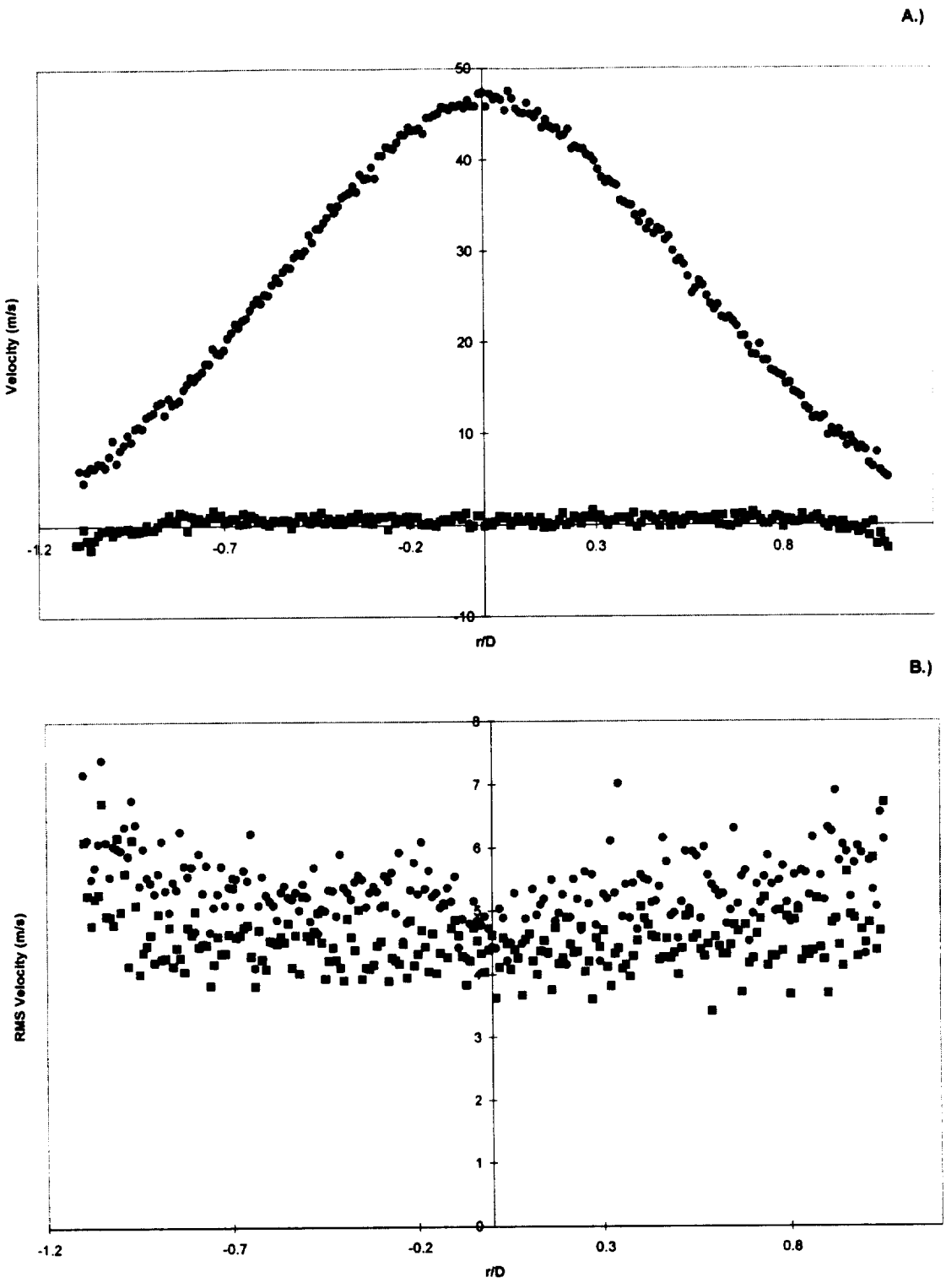

Fig. 9 2-Component PDV velocity results for standard jet; x/D = 6;
Circles-axial velocity; Squares-cicumferential velocity
a.) mean velocities
b.) RMS velocities

10-1-99

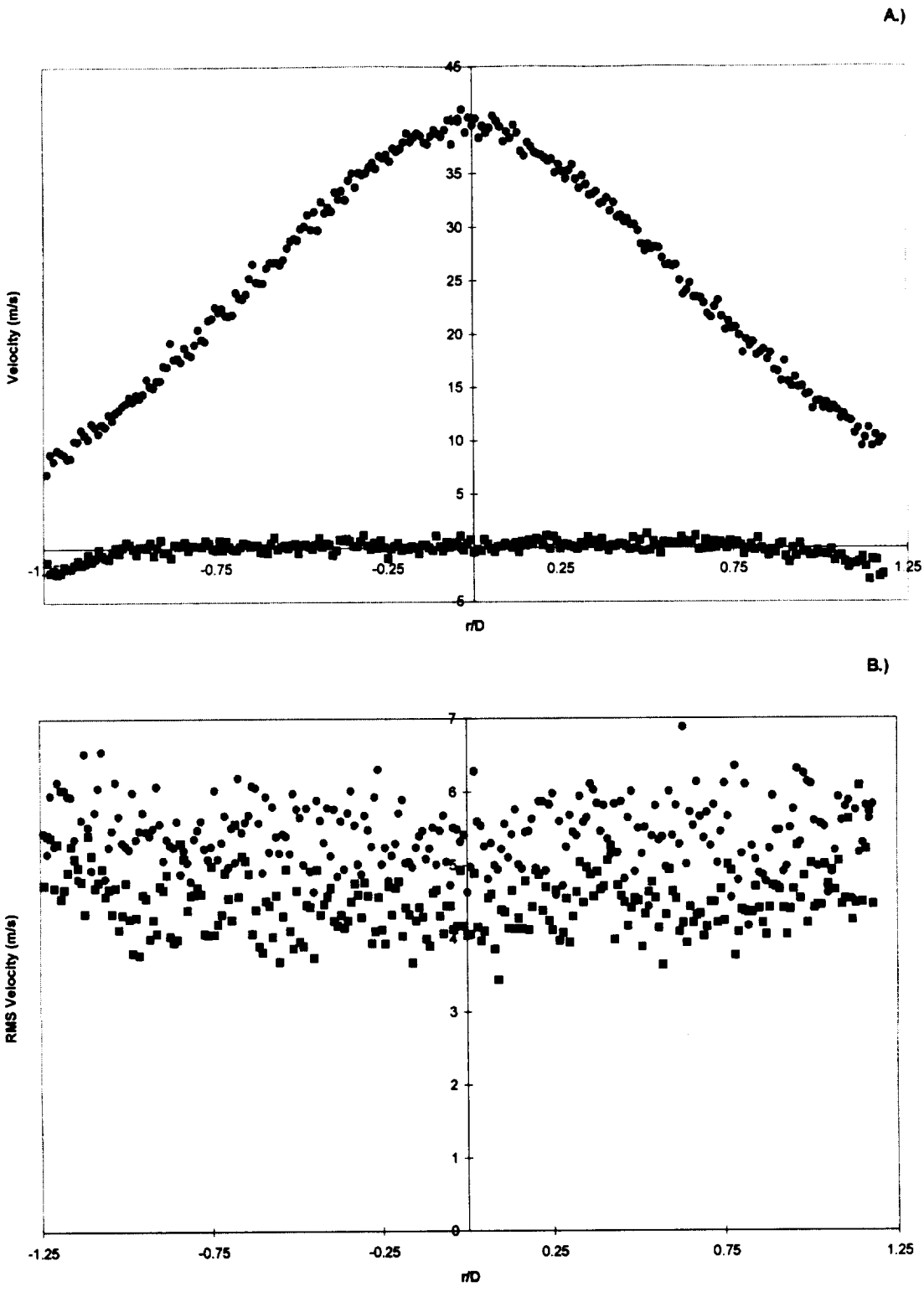

Fig. 10 2-Component PDV velocity results for standard jet; x/D = 8;
Circles-axial velocity; Squares-cicumferential velocity
a.) mean velocities
b.) RMS velocities

10-1-99

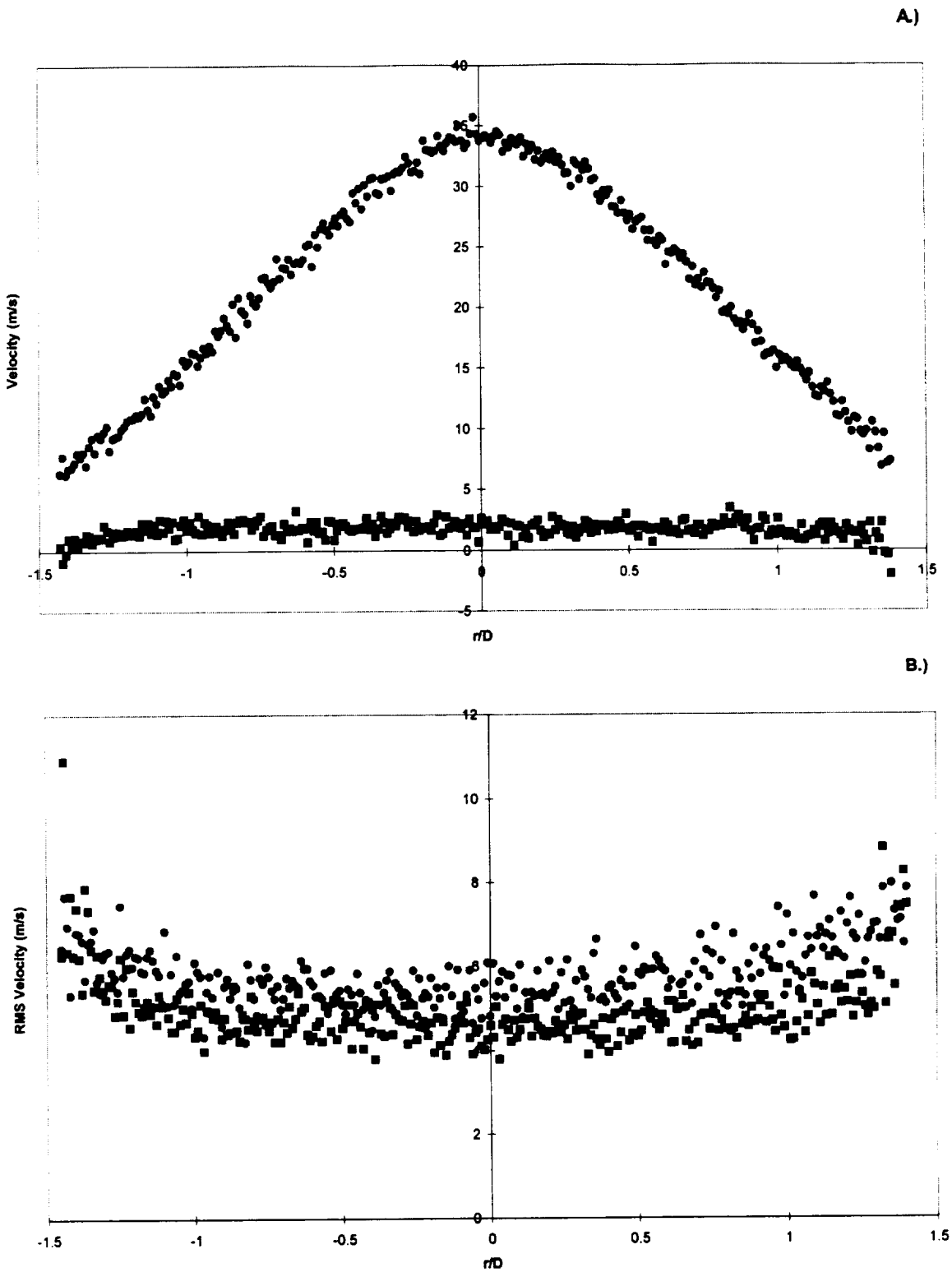

Fig. 11 2-Component PDV velocity results for standard jet; x/D = 10;
Circles-axial velocity; Squares-cicumferential velocity
a.) mean velocities
b.) RMS velocities

10-1-99

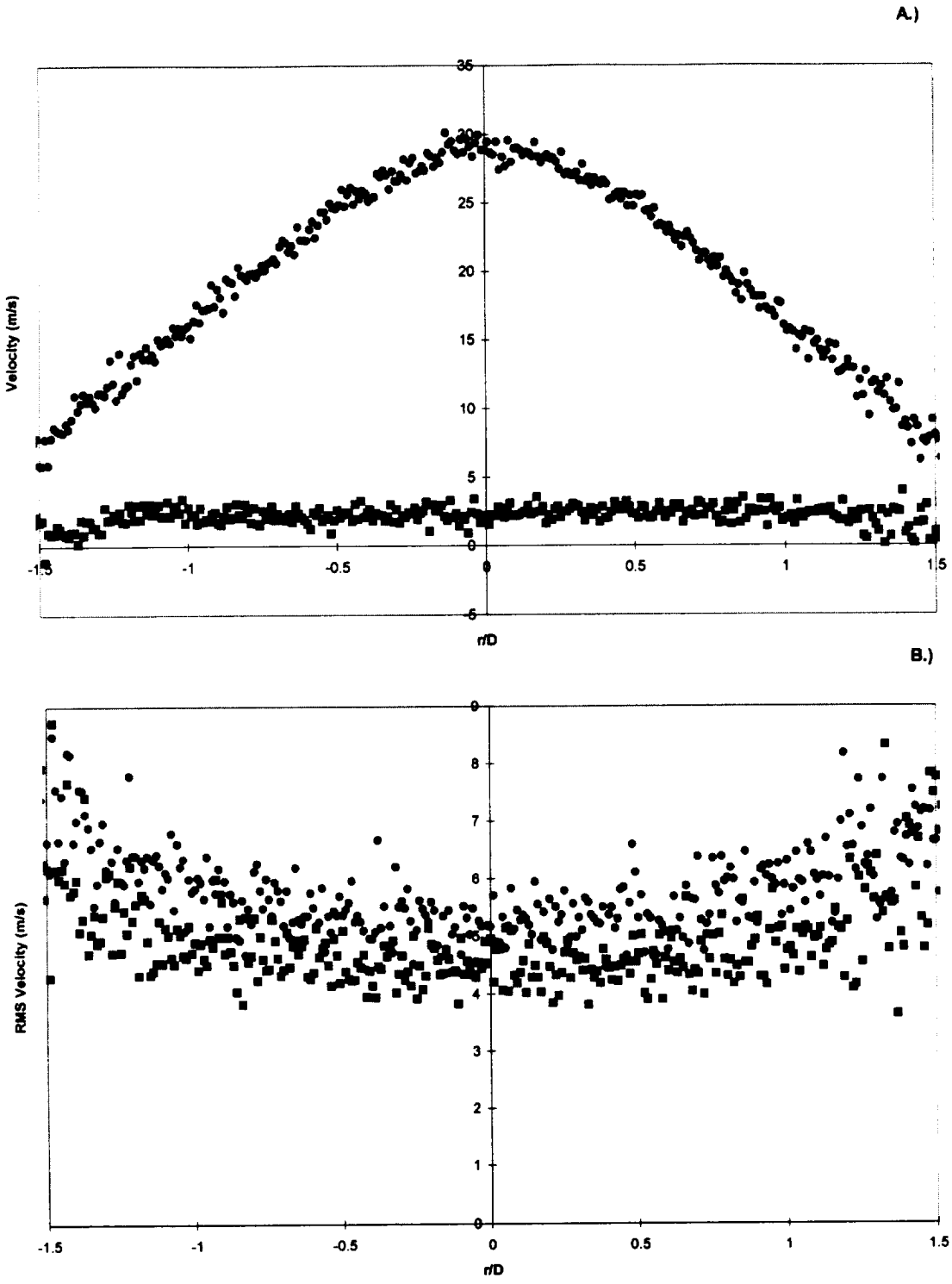

Fig. 12 2-Component PDV velocity results for standard jet; x/D = 12;
Circles-axial velocity; Squares-circumferential velocity
a.) mean velocities
b.) RMS velocities

10-1-99

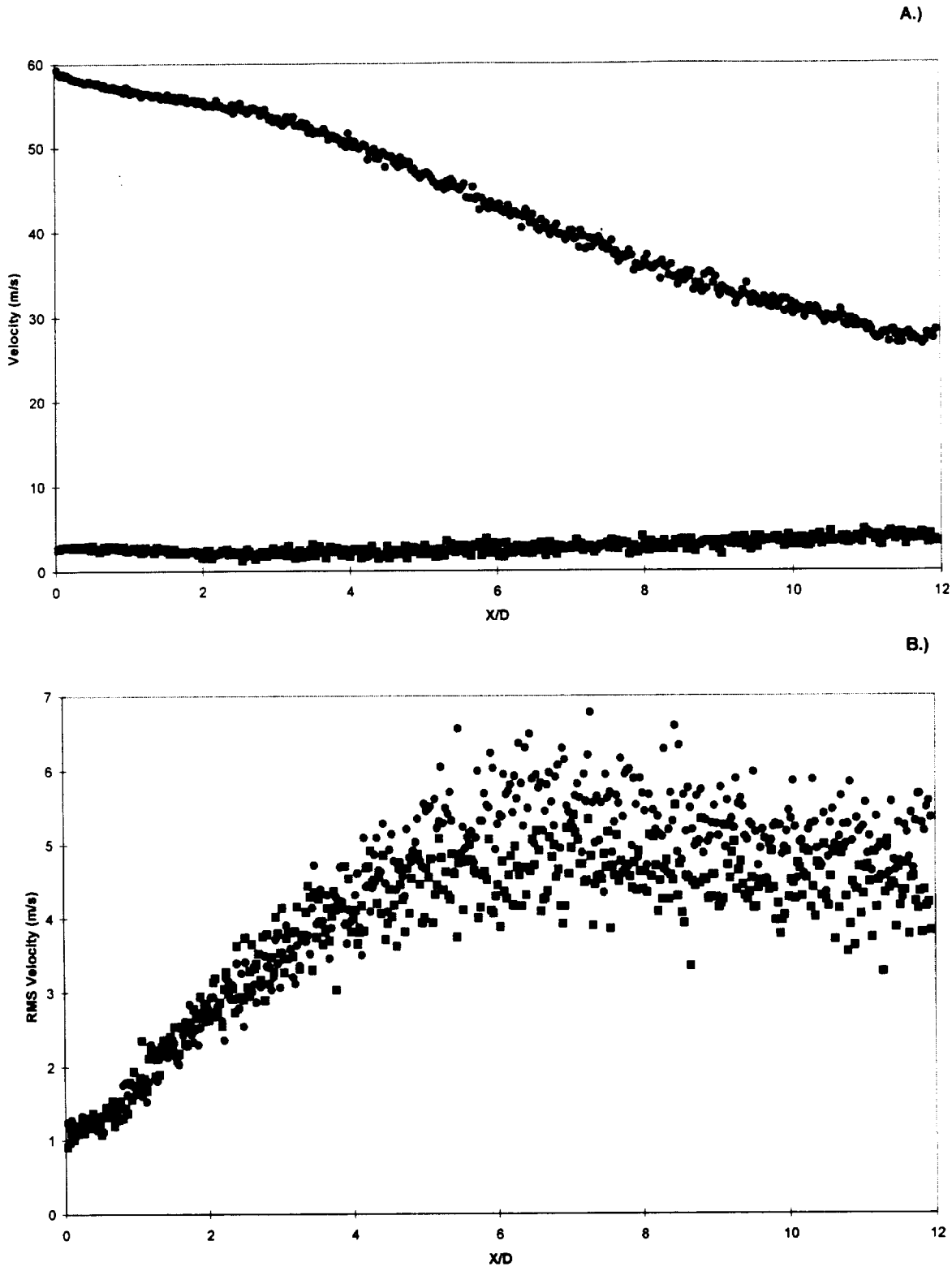

Fig. 13 2-Component PDV velocity results for standard jet; Centerline; Circles-axial velocity; Squares-circumferential velocity
a.) mean velocities
b.) RMS velocities

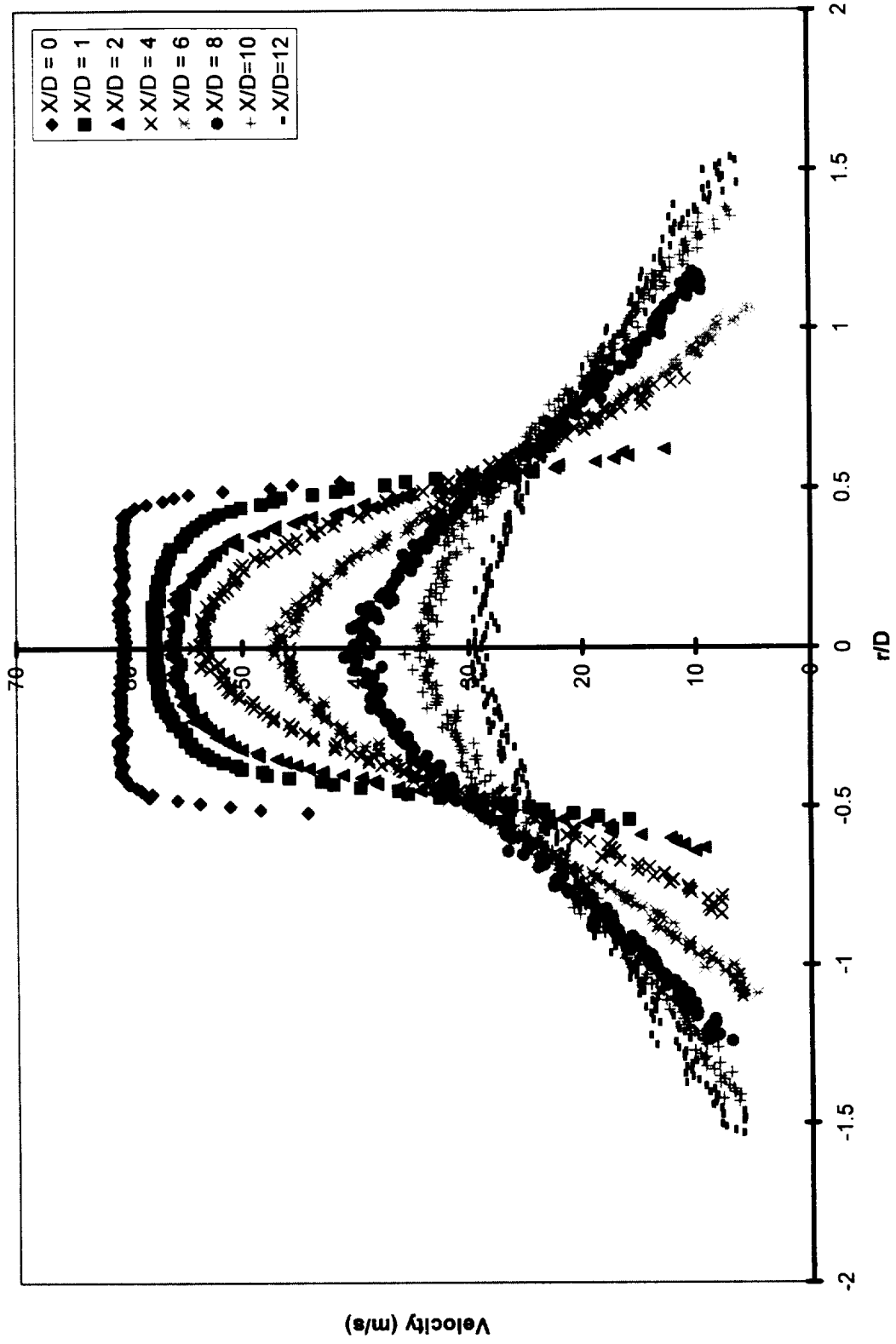

Fig. 14 Composite plot of PDV axial mean velocities for standard jet; Run 2

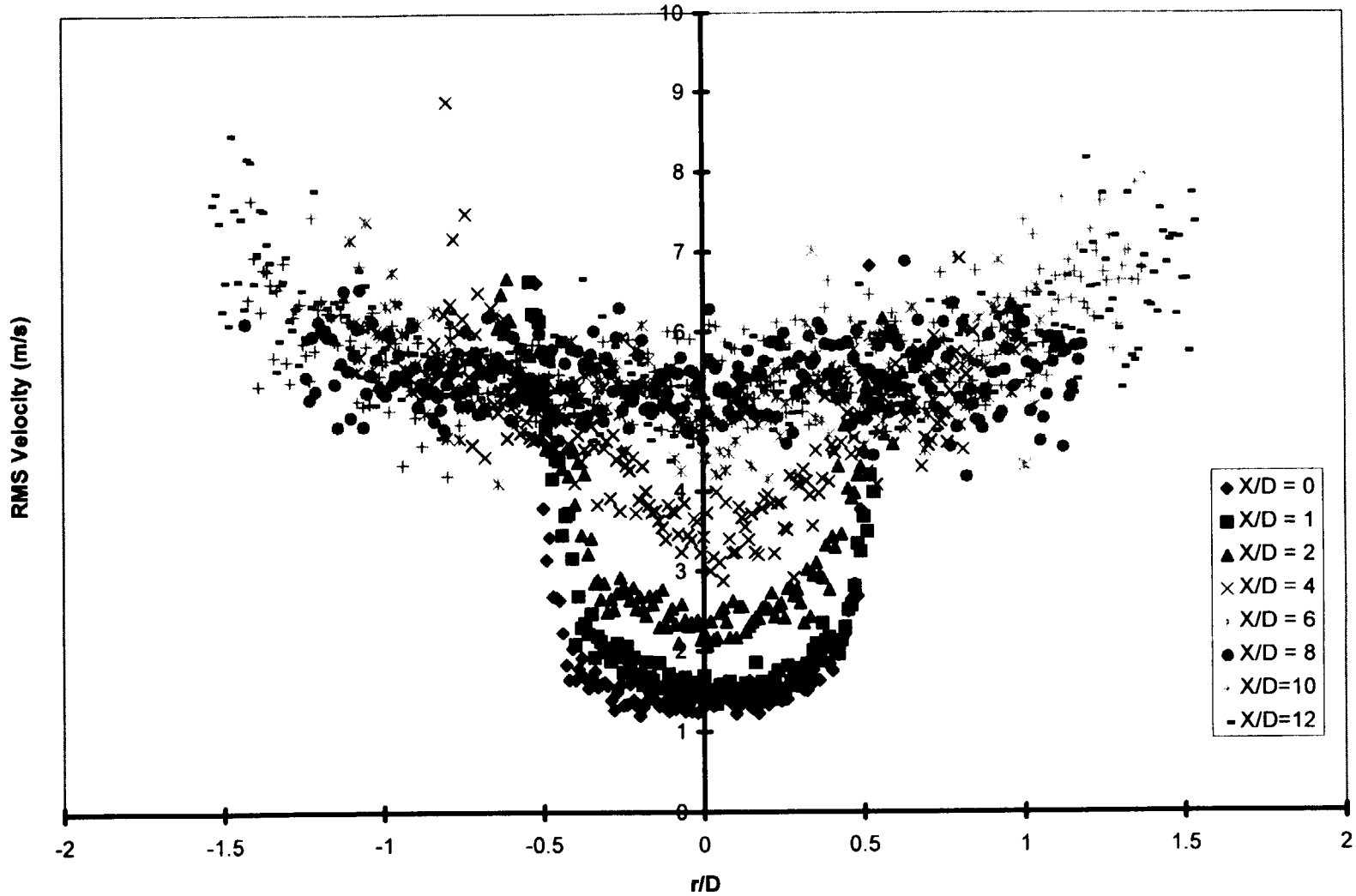

Fig. 15 Composite plot of PDV axial RMS velocities for standard jet; Run 2

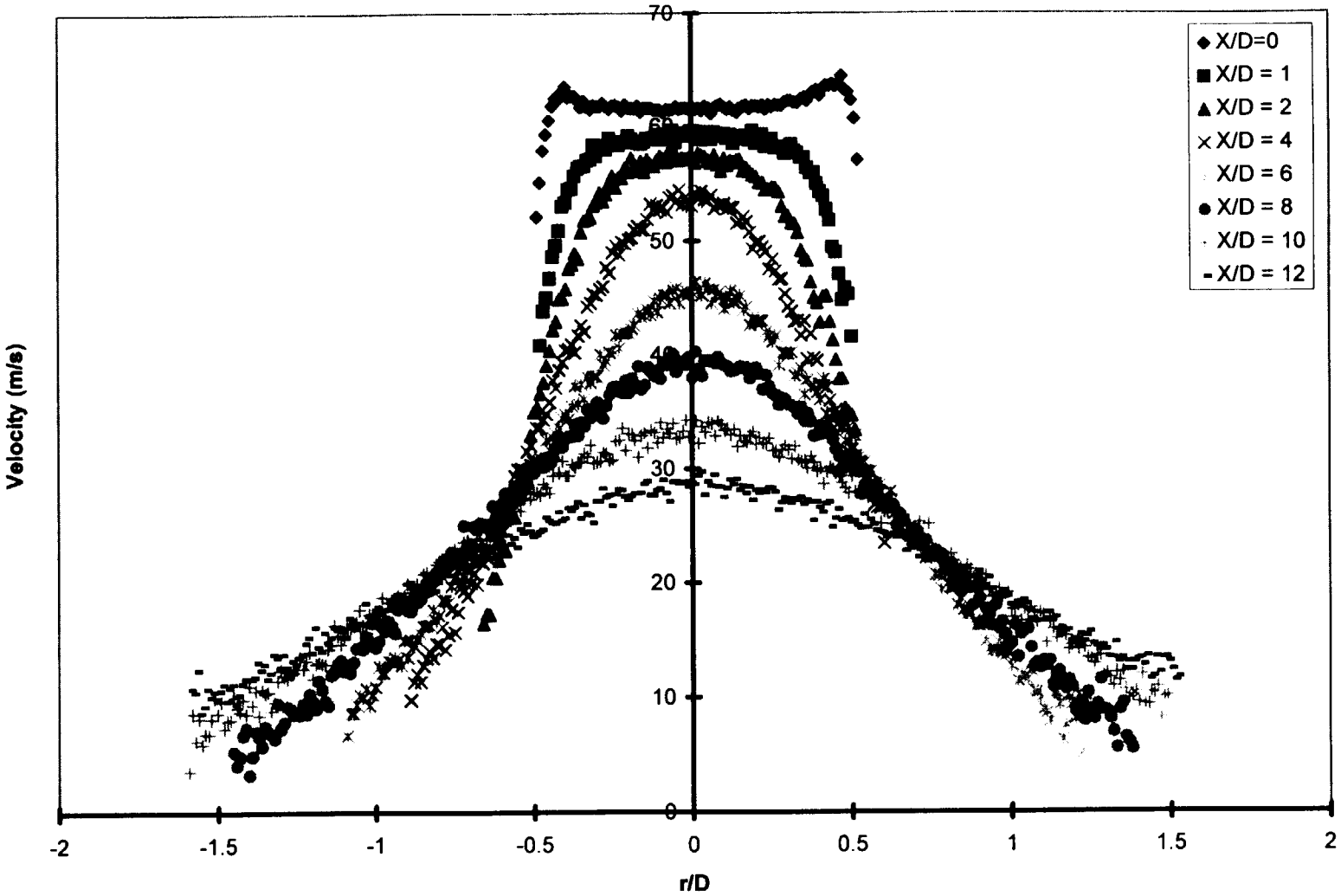

Fig. 16 Composite plot of PDV axial mean velocities for standard jet; Run 1

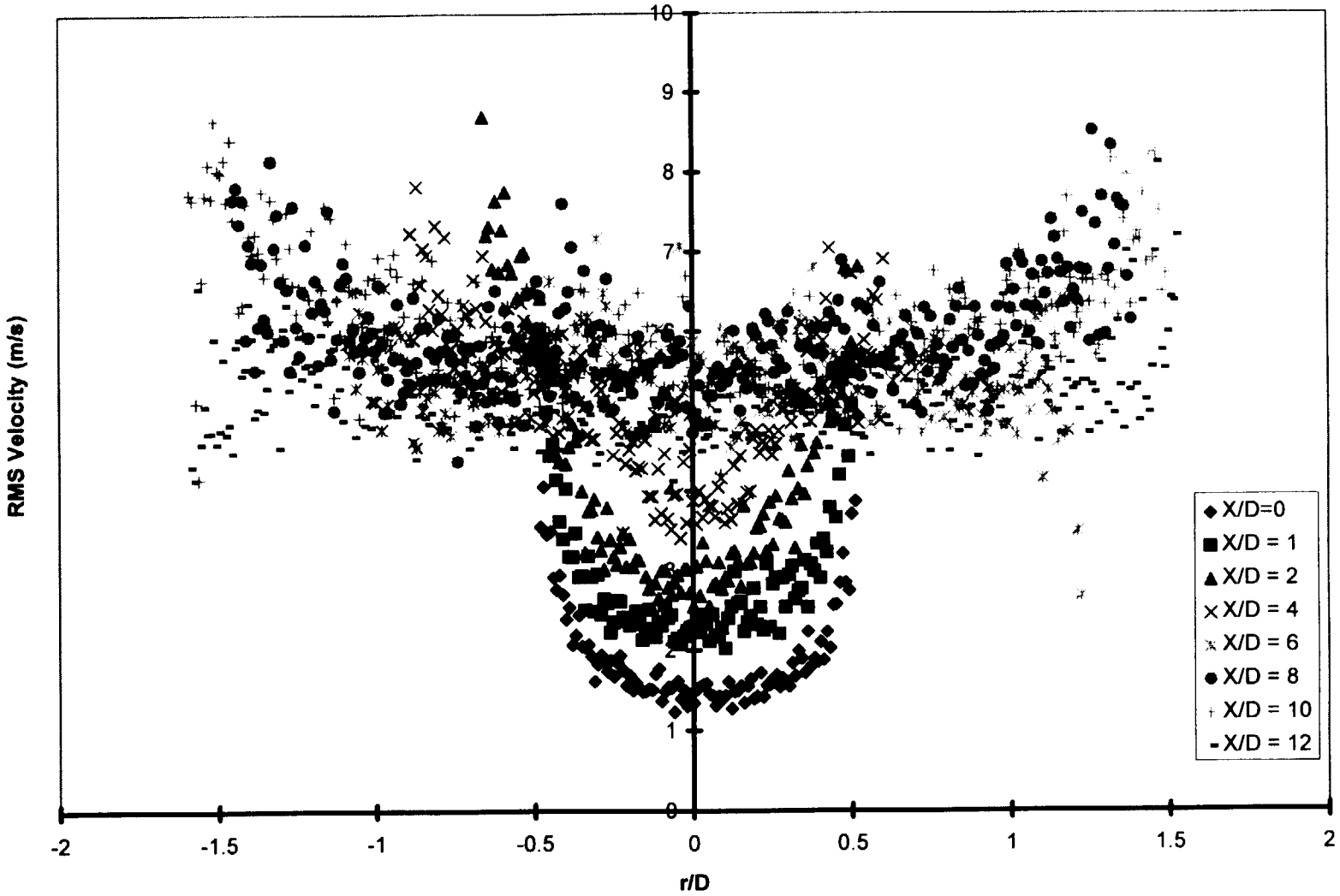

Fig. 17 Composite plot of PDV axial RMS velocities for standard jet; Run 1

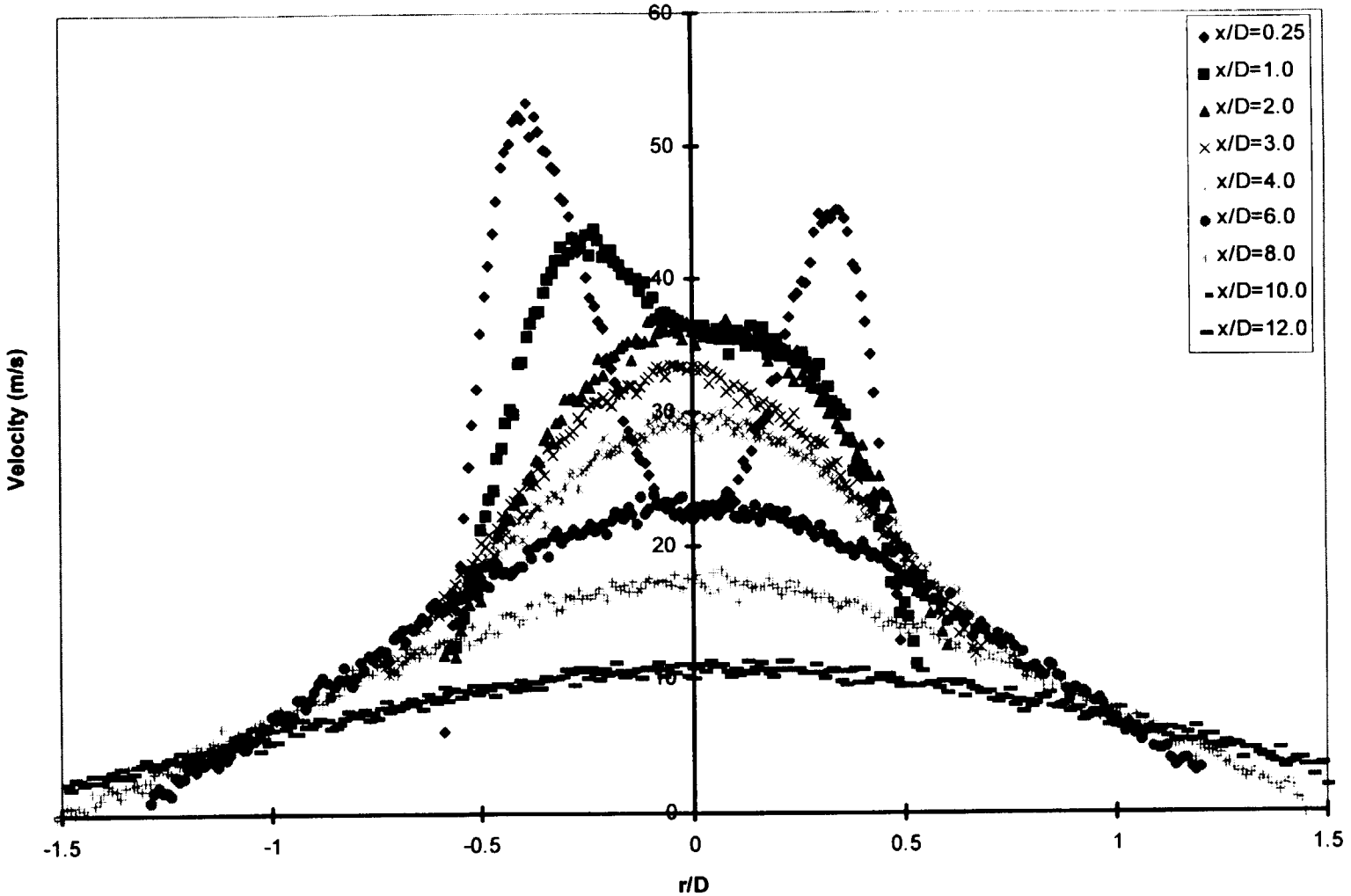

Fig. 18 Composite plot of PDV axial mean velocities for annular jet; Run 1

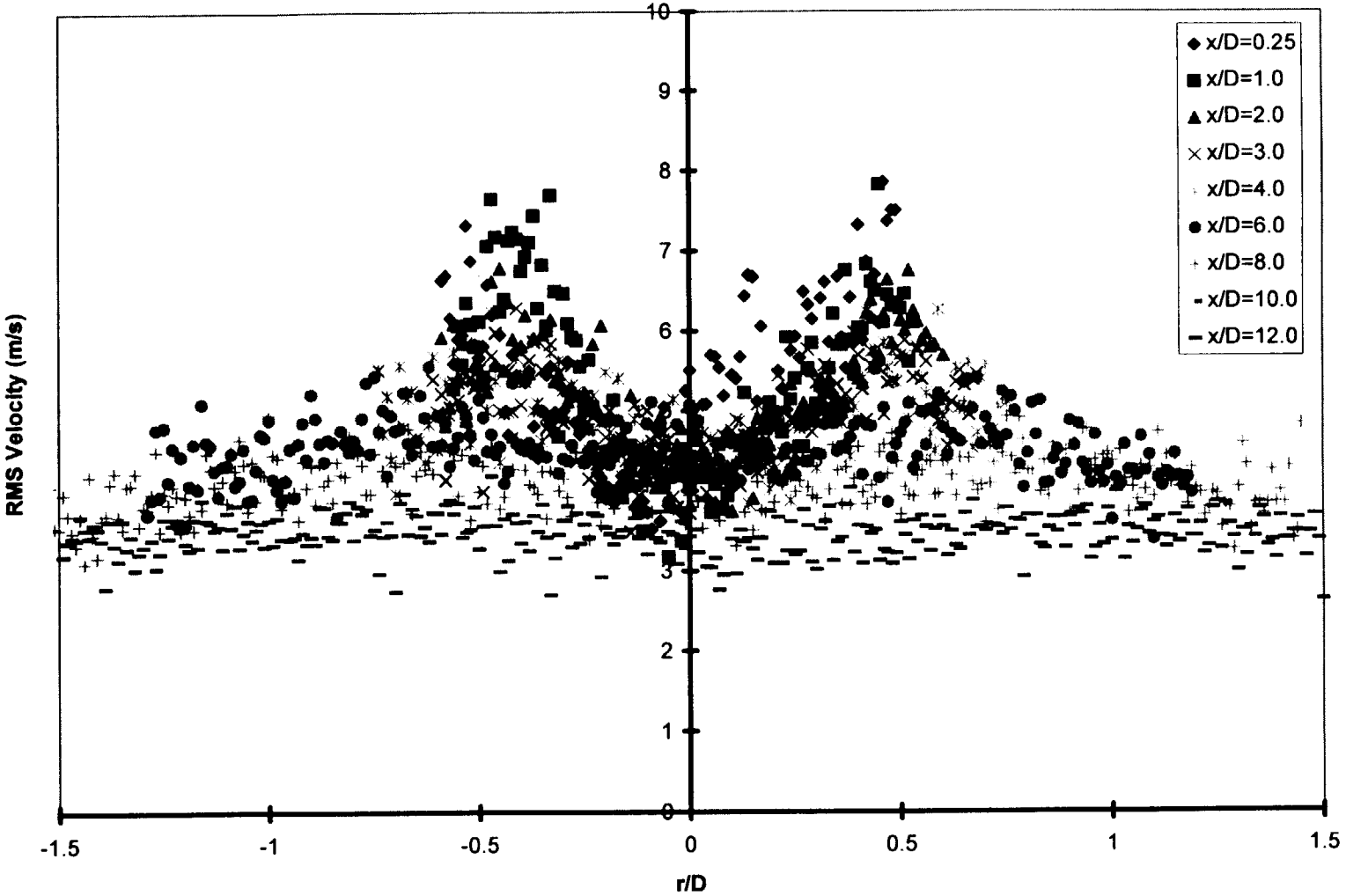

Fig. 19 Composite plot of PDV axial RMS velocities for annular jet; Run 1

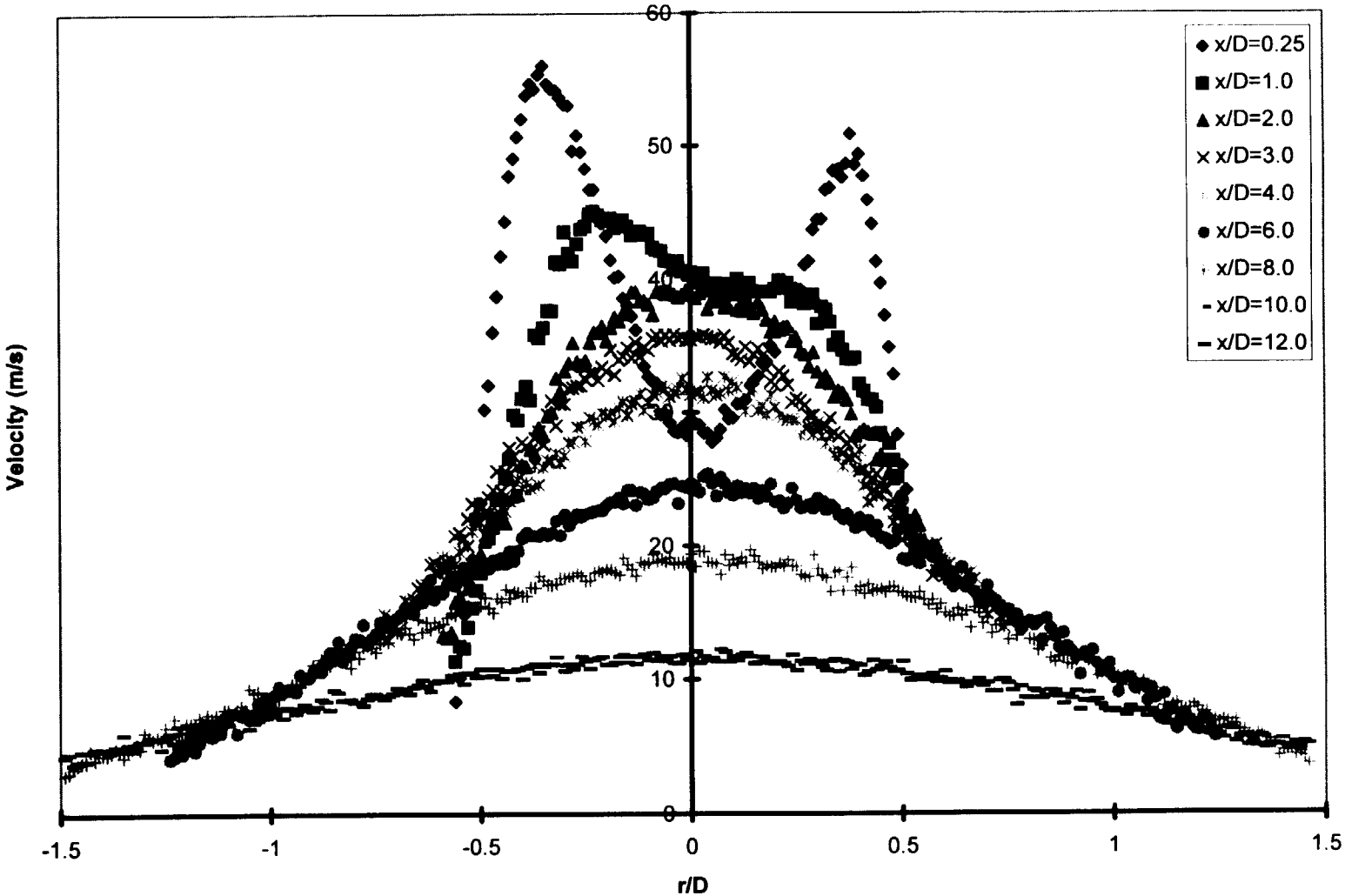

Fig. 20 Composite plot of PDV axial mean velocities for annular jet; Run 2

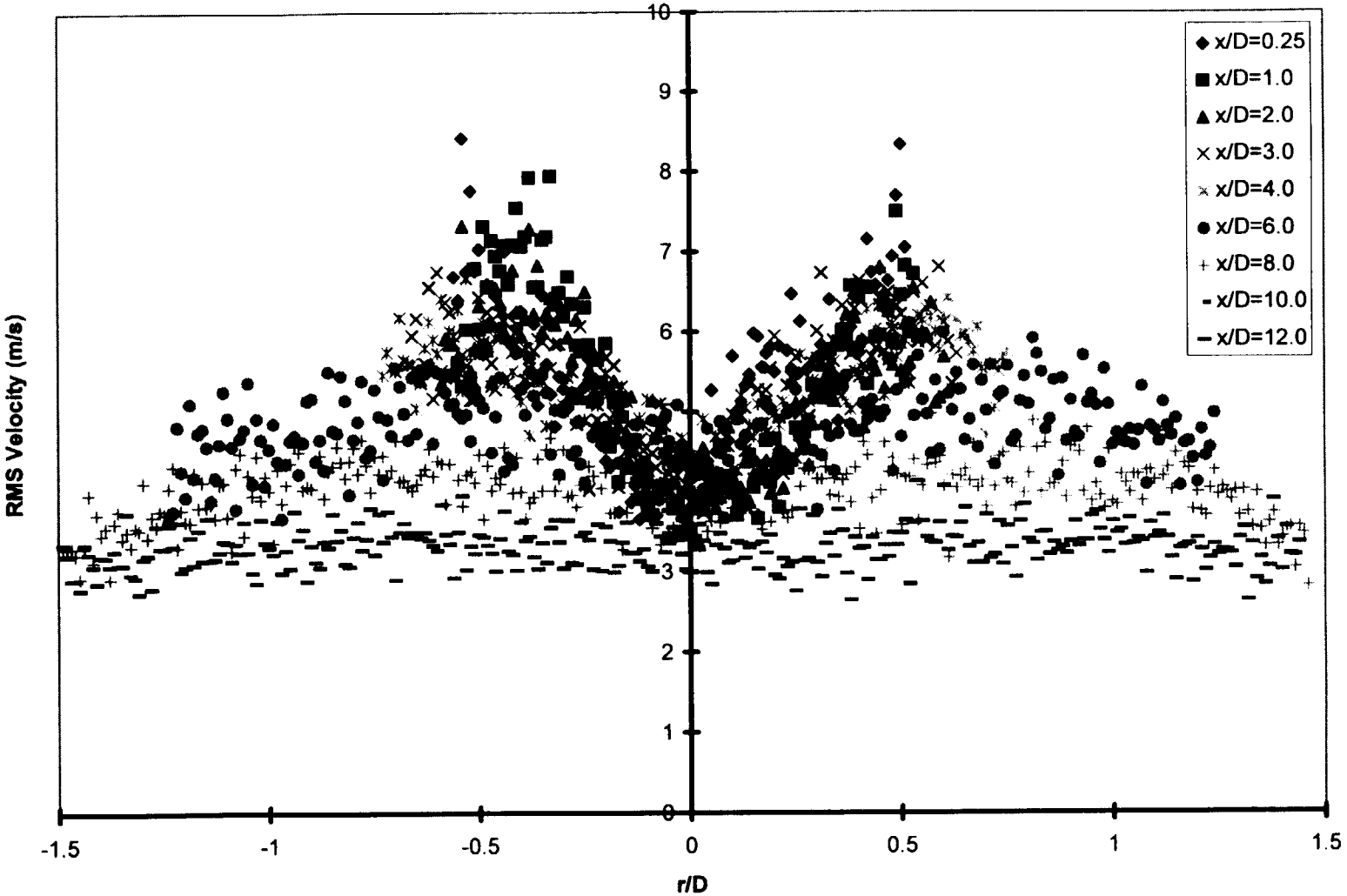

Fig. 21 Composite plot of PDV axial RMS velocities for annular jet; Run 2

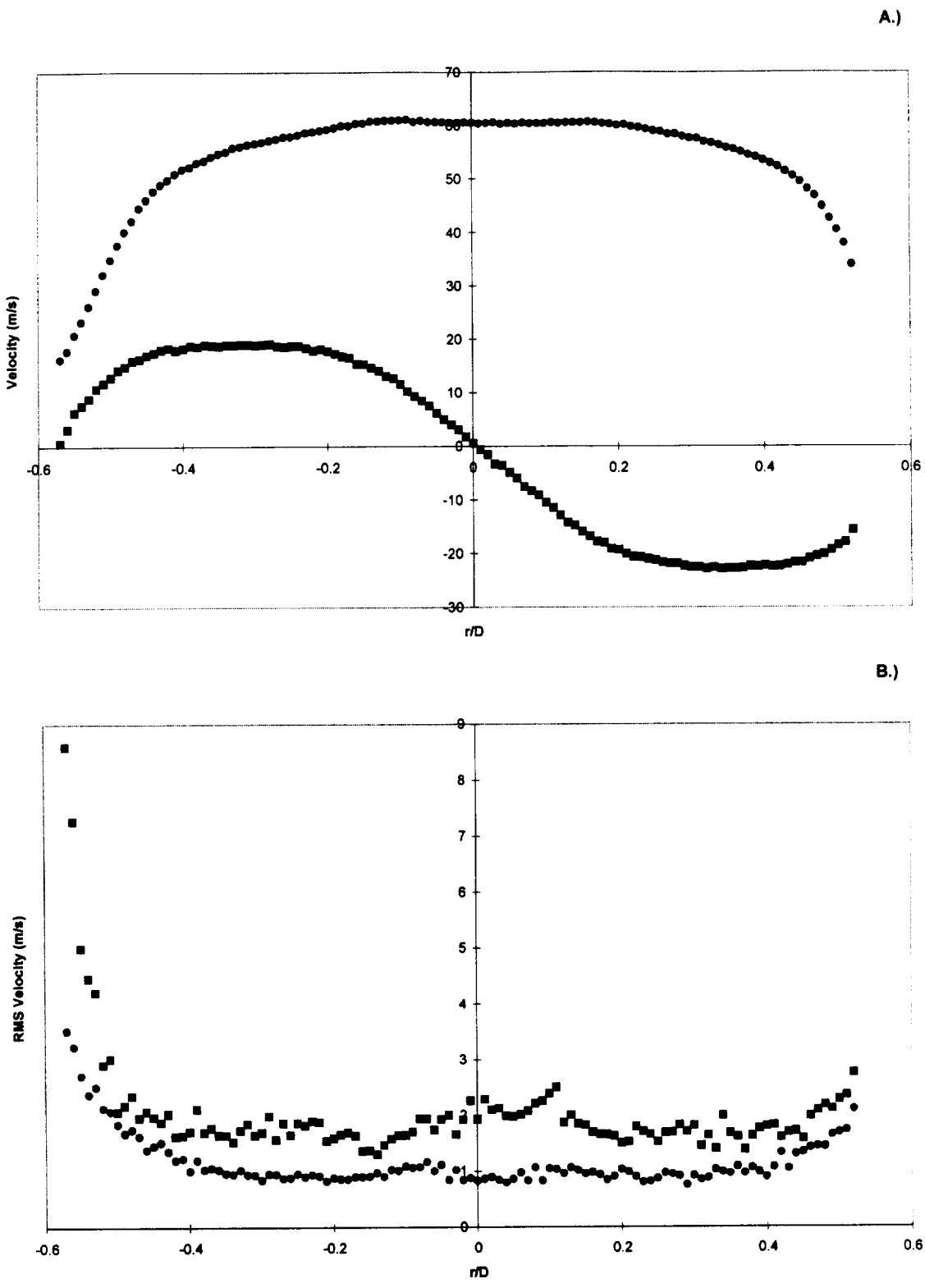

Fig. 22 2-Component PDV velocity results for swirling jet; x/D = 0.25;
Circles-axial velocity; Squares-circumferential velocity
a.) mean velocities
b.) RMS velocities

3-14-2000

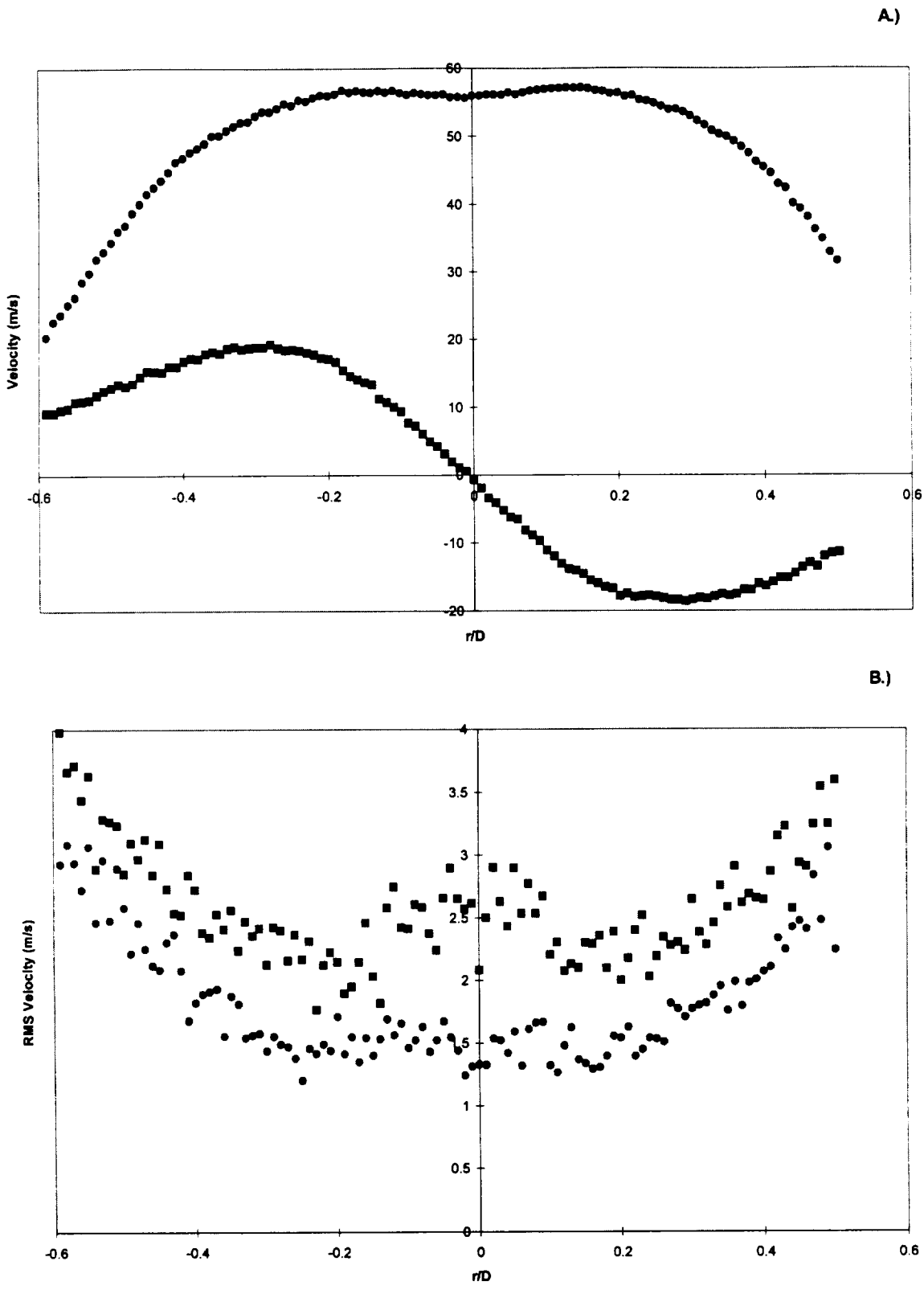

Fig. 23 2-Component PDV velocity results for swirling jet; x/D = 1;
Circles-axial velocity; Squares-circumferential velocity
a.) mean velocities
b.) RMS velocities

3-14-2000

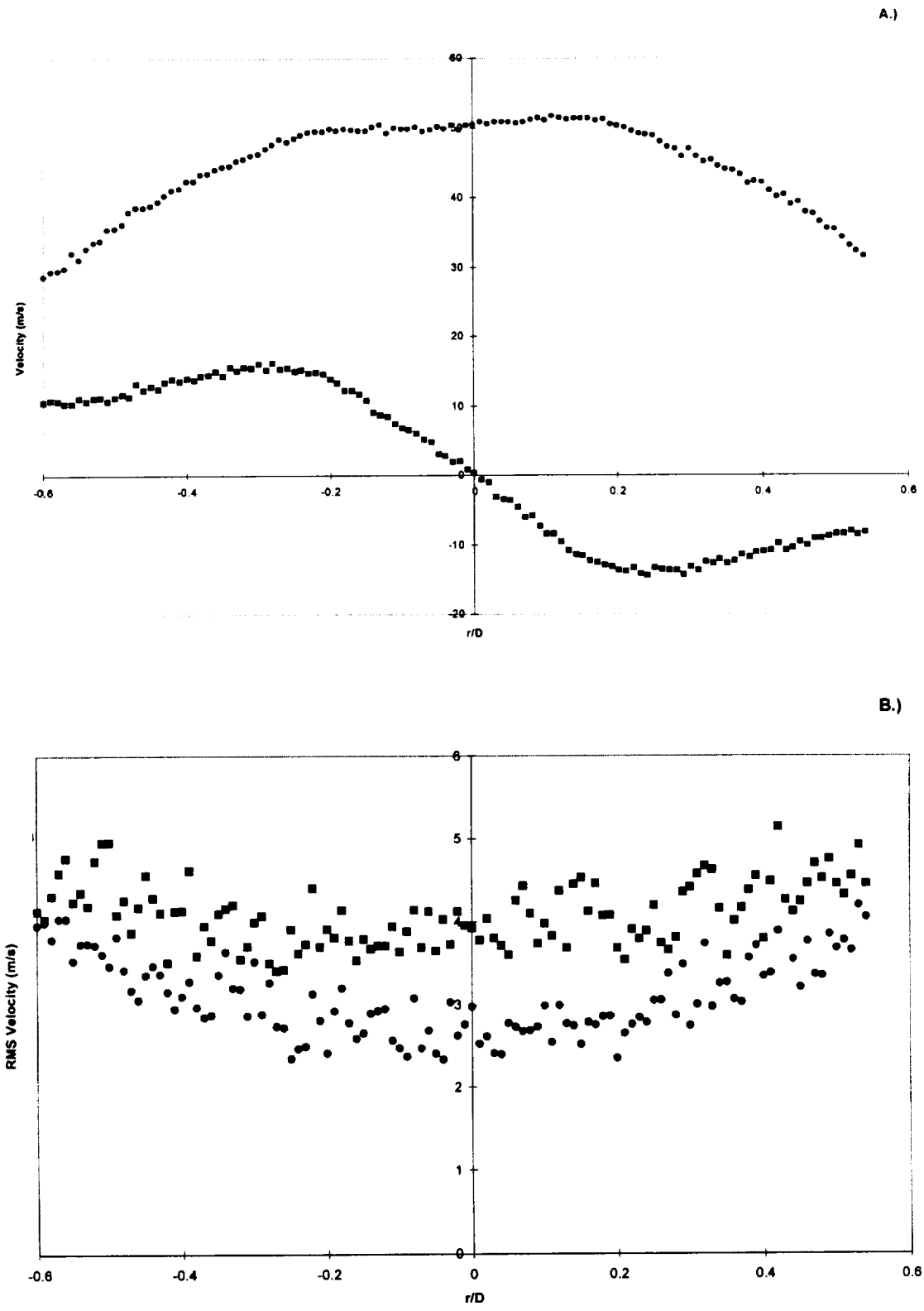

Fig. 24 2-Component PDV velocity results for swirling jet; x/D = 2;
Circles-axial velocity; Squares-circumferential velocity
a.) mean velocities
b.) RMS velocities

3-14-2000

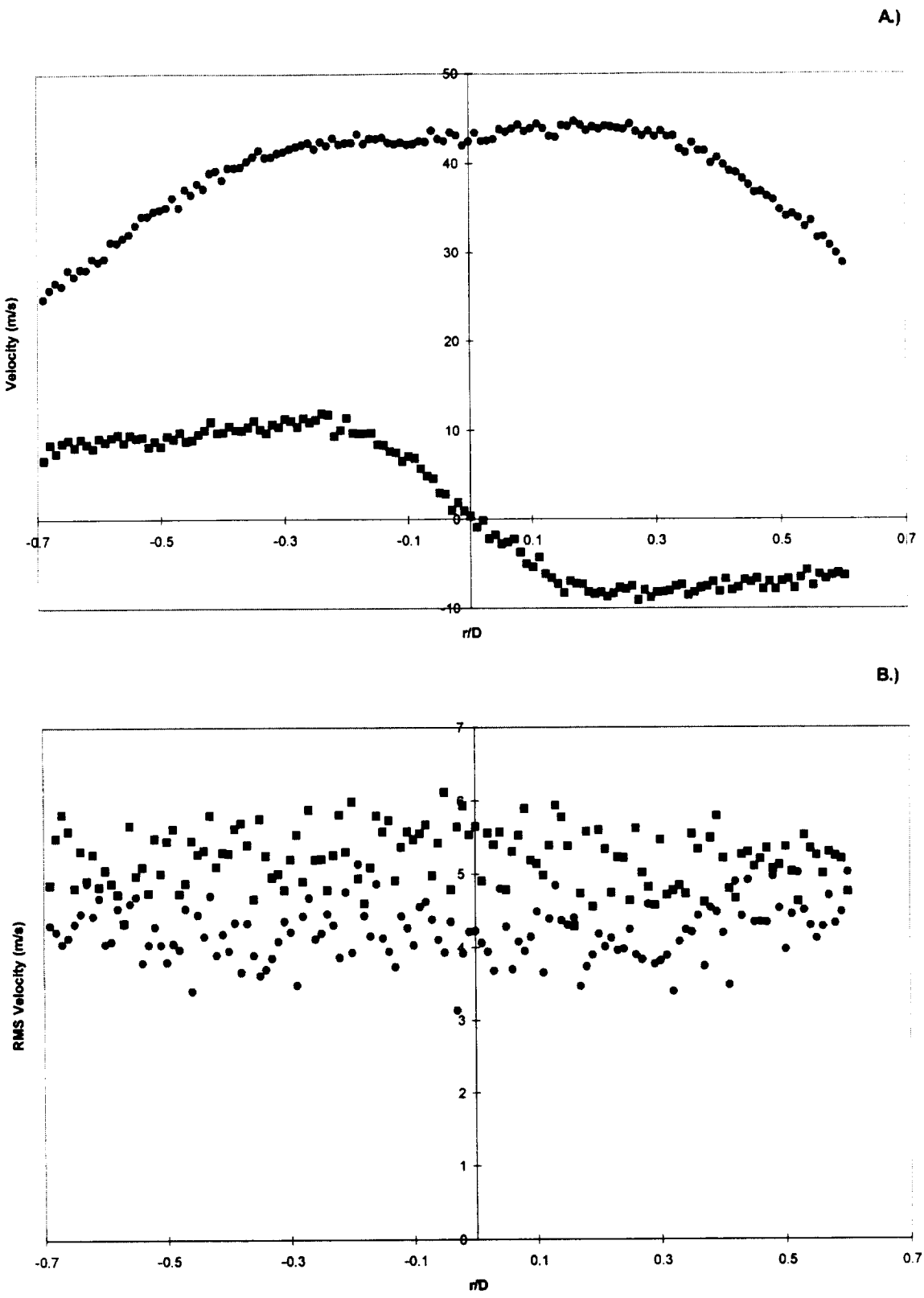

Fig. 25 2-Component PDV velocity results for swirling jet; x/D = 3;
Circles-axial velocity; Squares-circumferential velocity
a.) mean velocities
b.) RMS velocities

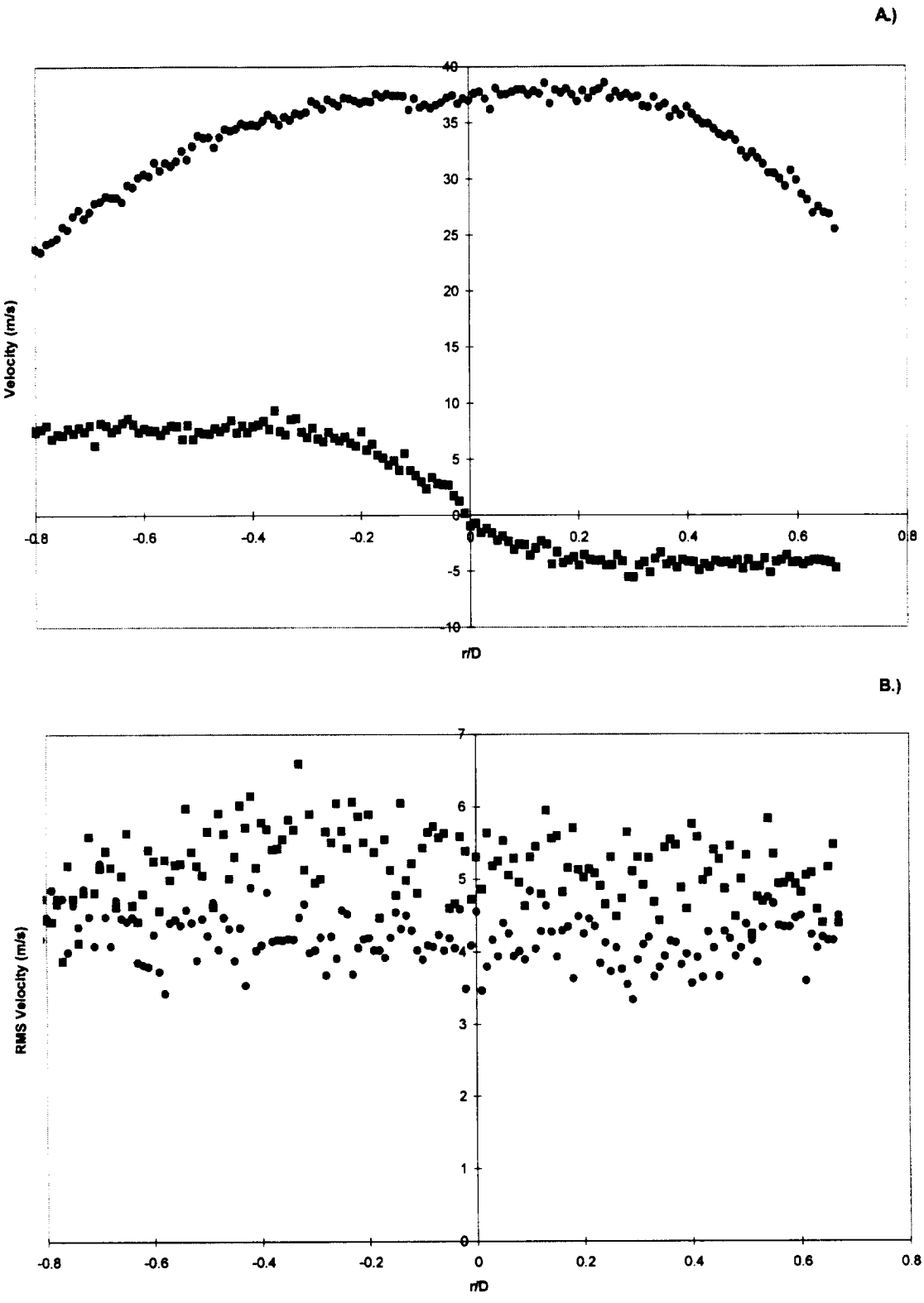

Fig. 26 2-Component PDV velocity results for swirling jet; x/D = 4;
Circles-axial velocity; Squares-circumferential velocity
a.) mean velocities
b.) RMS velocities

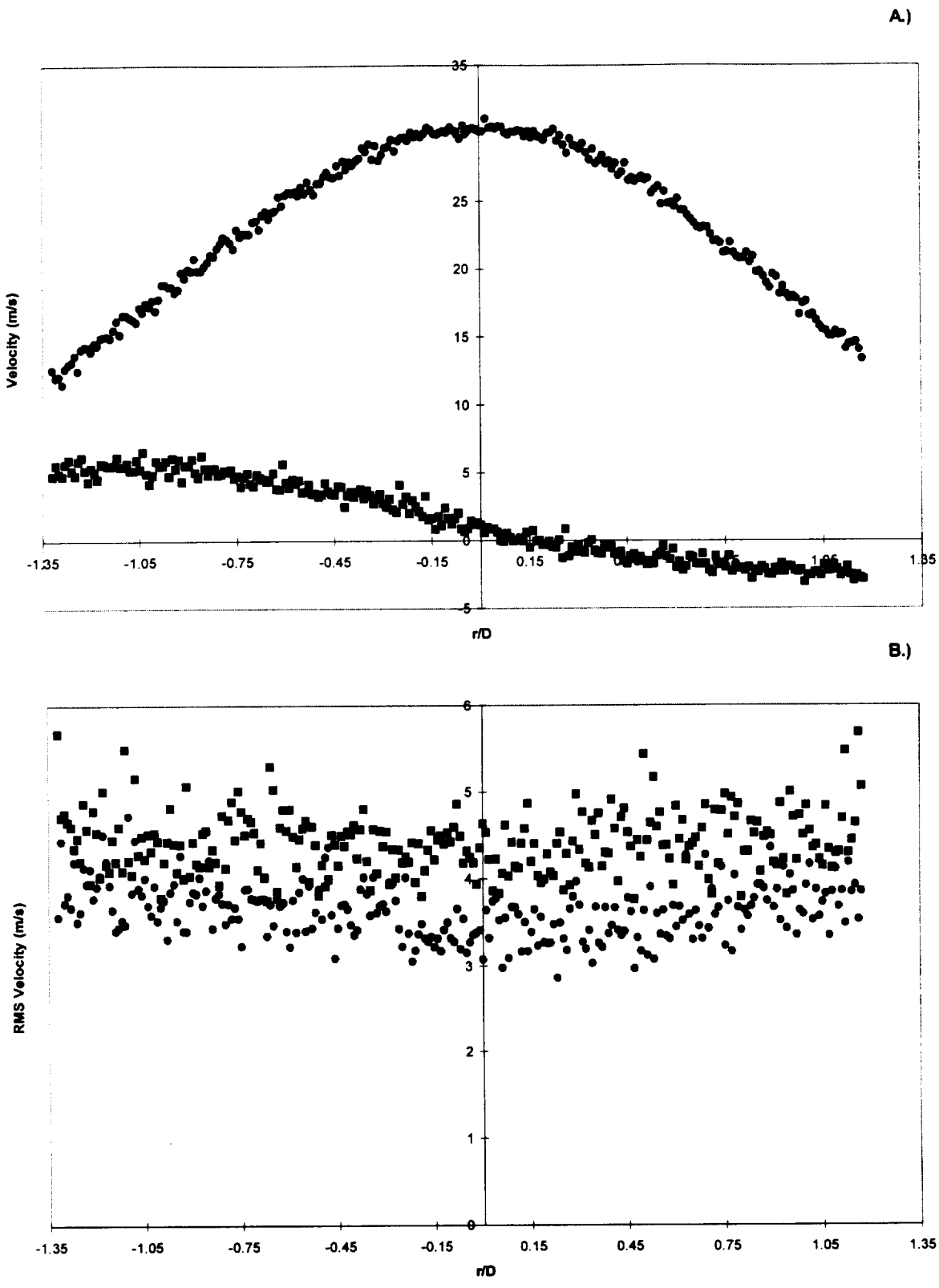

Fig. 27 2-Component PDV velocity results for swirling jet; x/D = 6;
Circles-axial velocity; Squares-circumferential velocity
a.) mean velocities
b.) RMS velocities

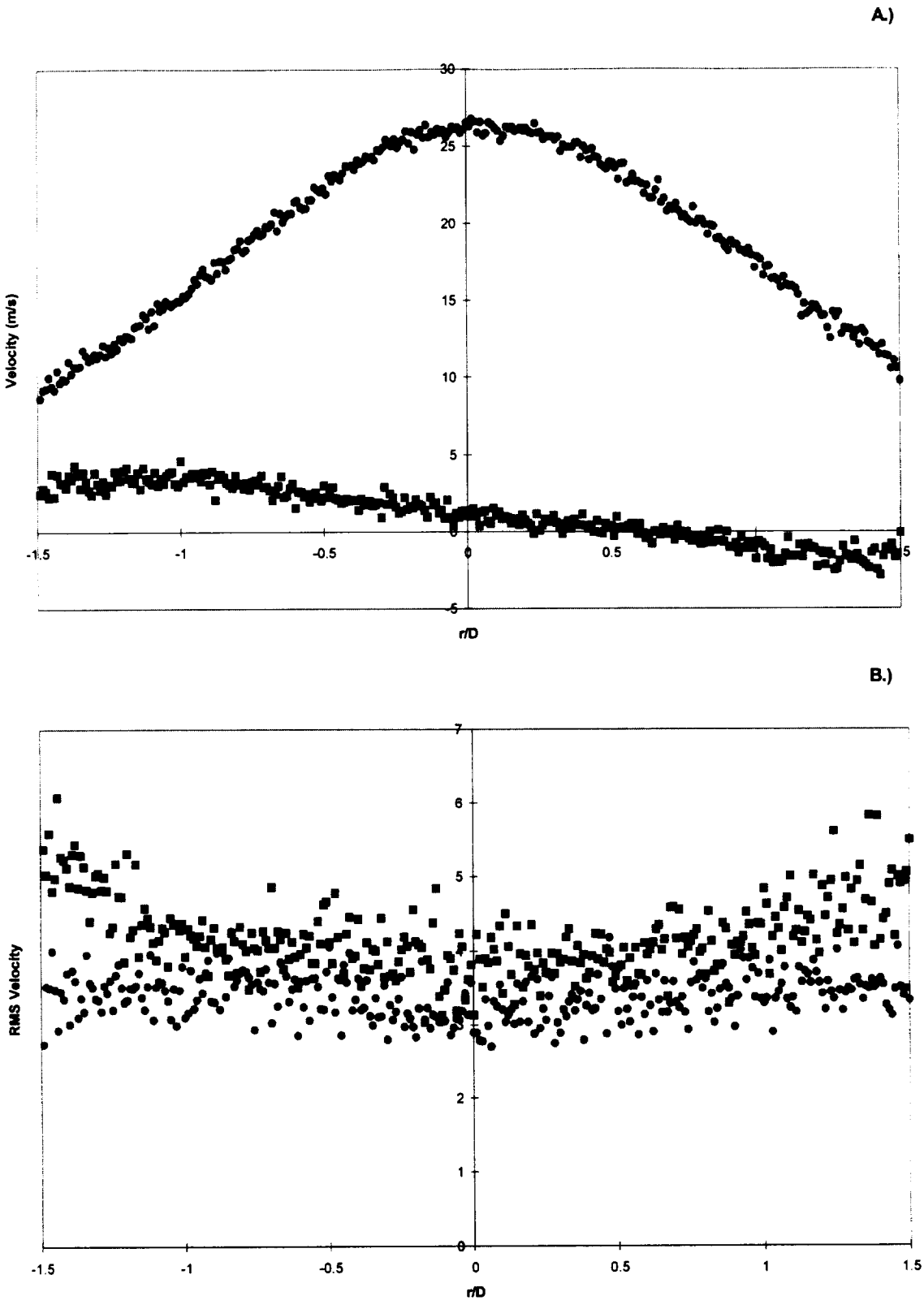

Fig. 28 2-Component PDV velocity results for swirling jet; x/D = 8;
Circles-axial velocity; Squares-circumferential velocity
a.) mean velocities
b.) RMS velocities

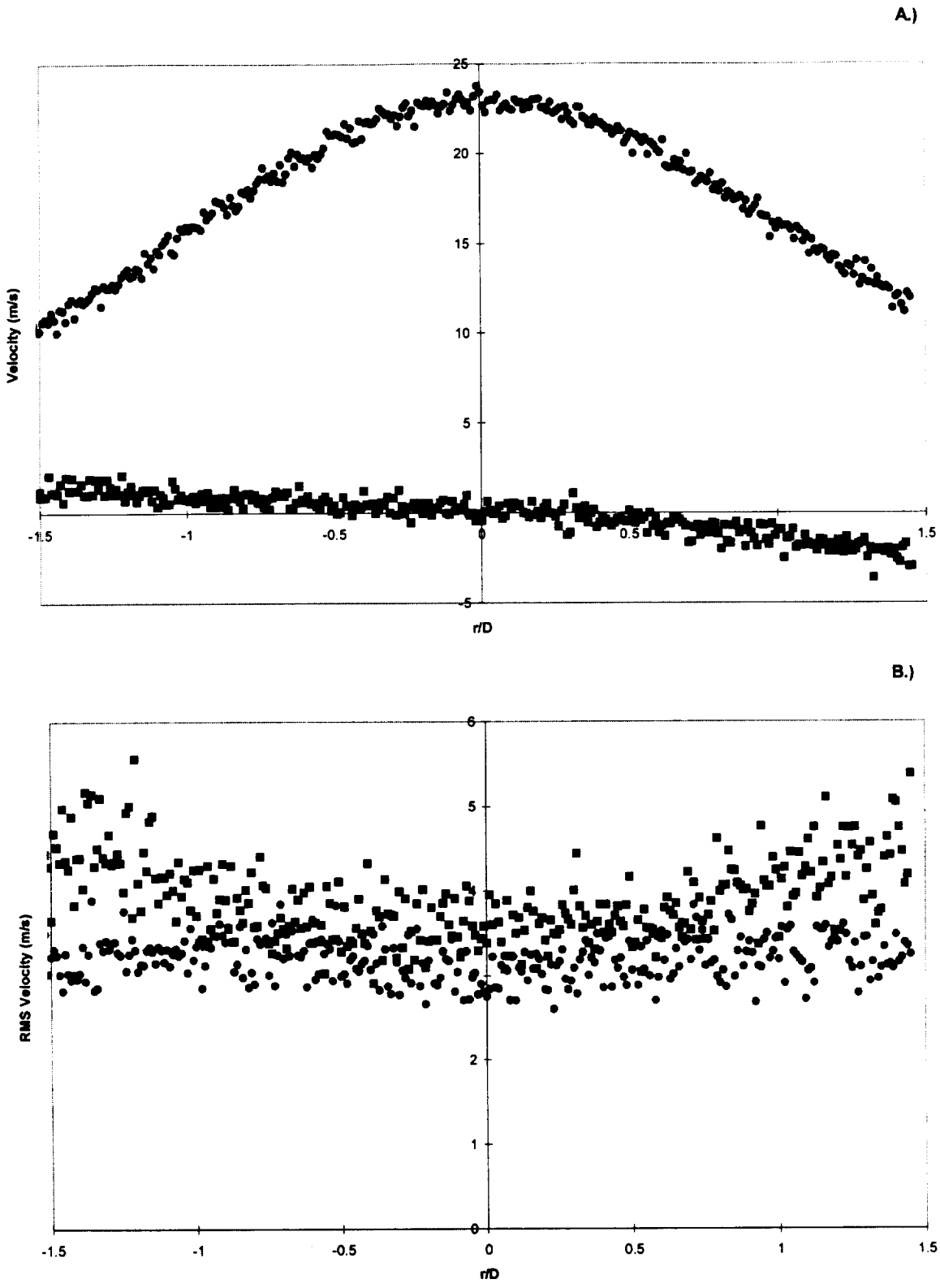

Fig. 29 2-Component PDV velocity results for swirling jet; x/D = 10;
Circles-axial velocity; Squares-circumferential velocity
a.) mean velocities
b.) RMS velocities

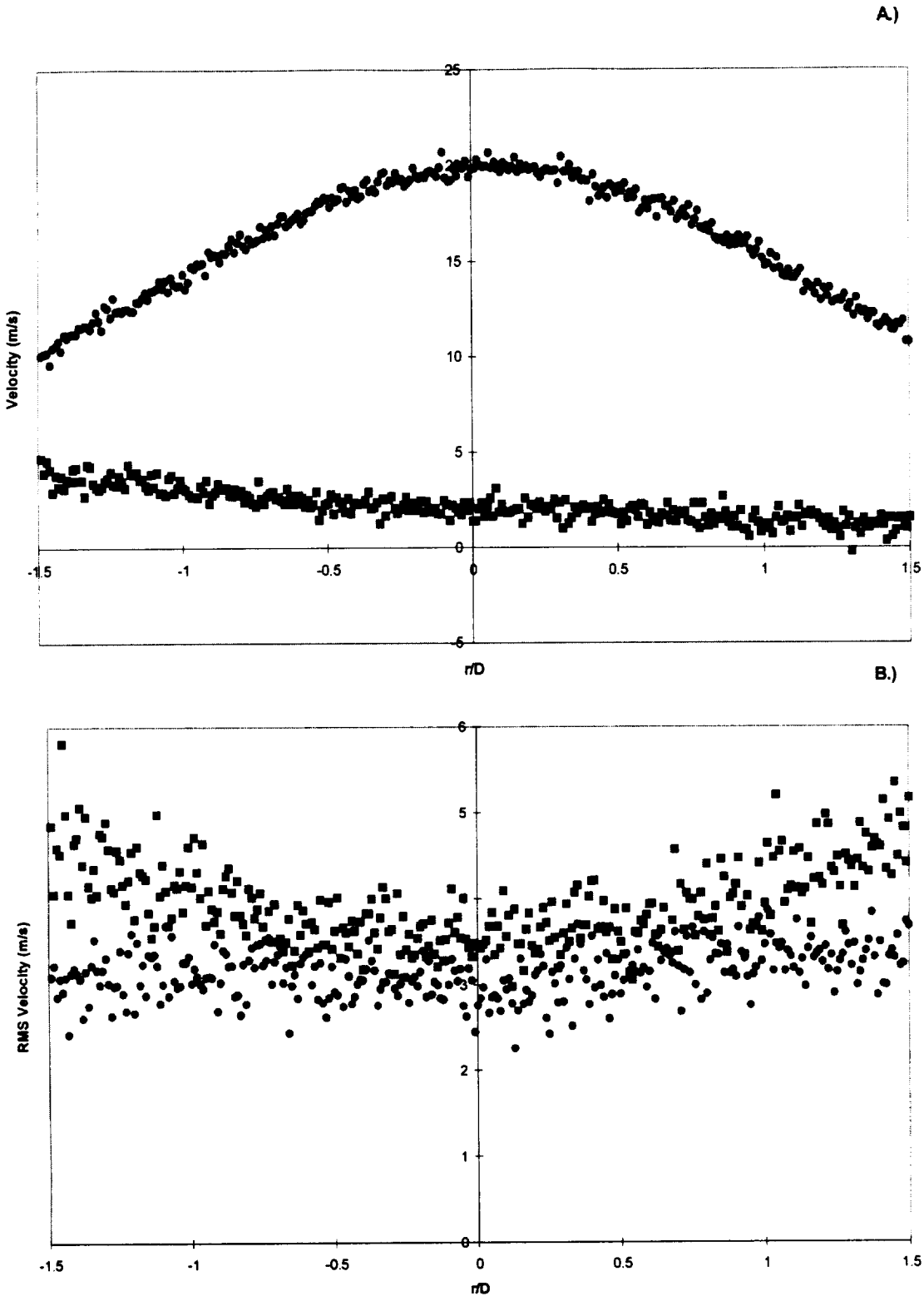

Fig. 30 2-Component PDV velocity results for swirling jet; x/D = 12;
Circles-axial velocity; Squares-circumferential velocity
a.) mean velocities
b.) RMS velocities

3-14-2000

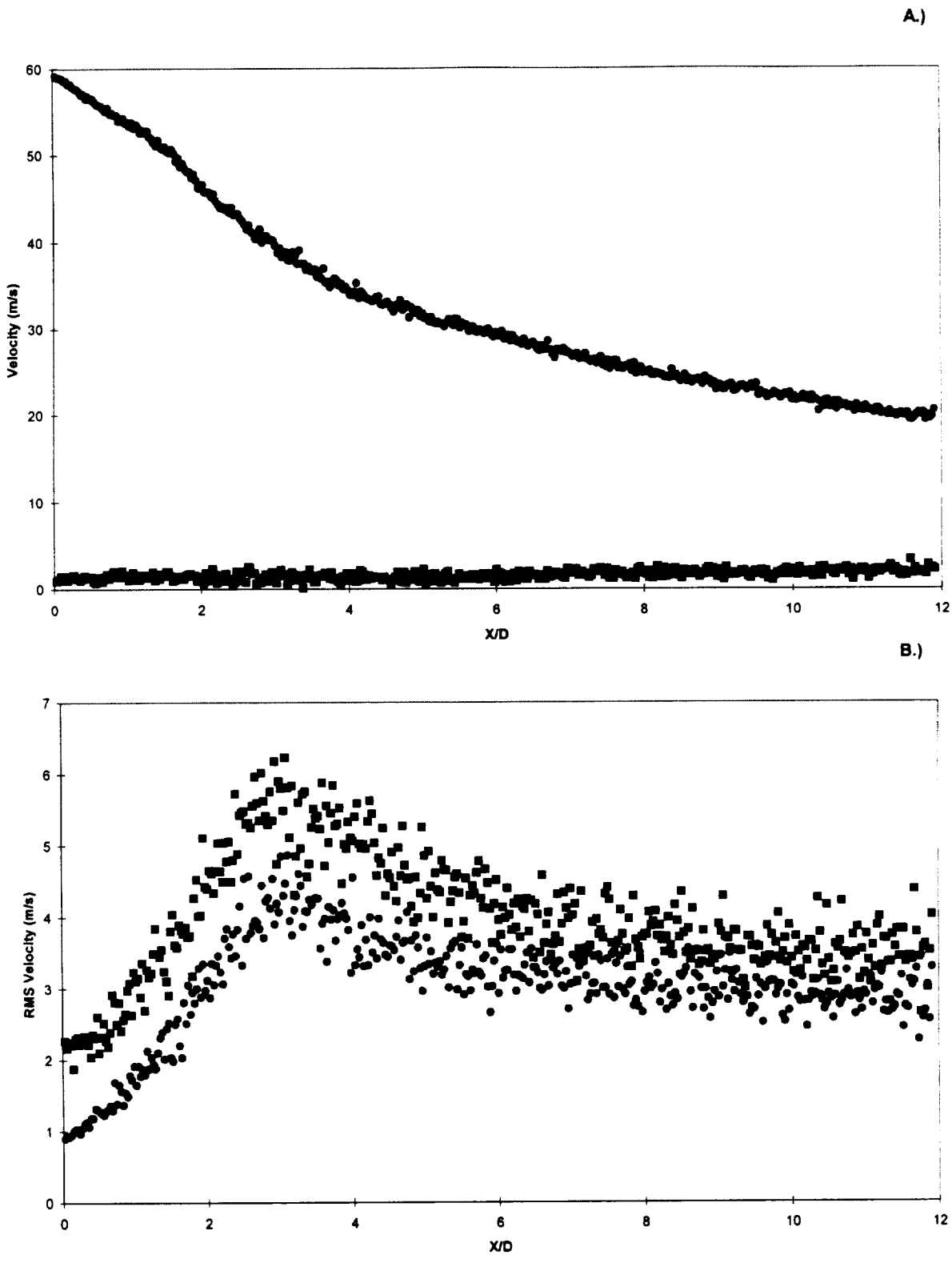

Fig. 31 2-Component PDV velocity results for swirling jet; Centerline; Circles-axial velocity; Squares-circumferential velocity
a.) mean velocities
b.) RMS velocities

3-14-2000

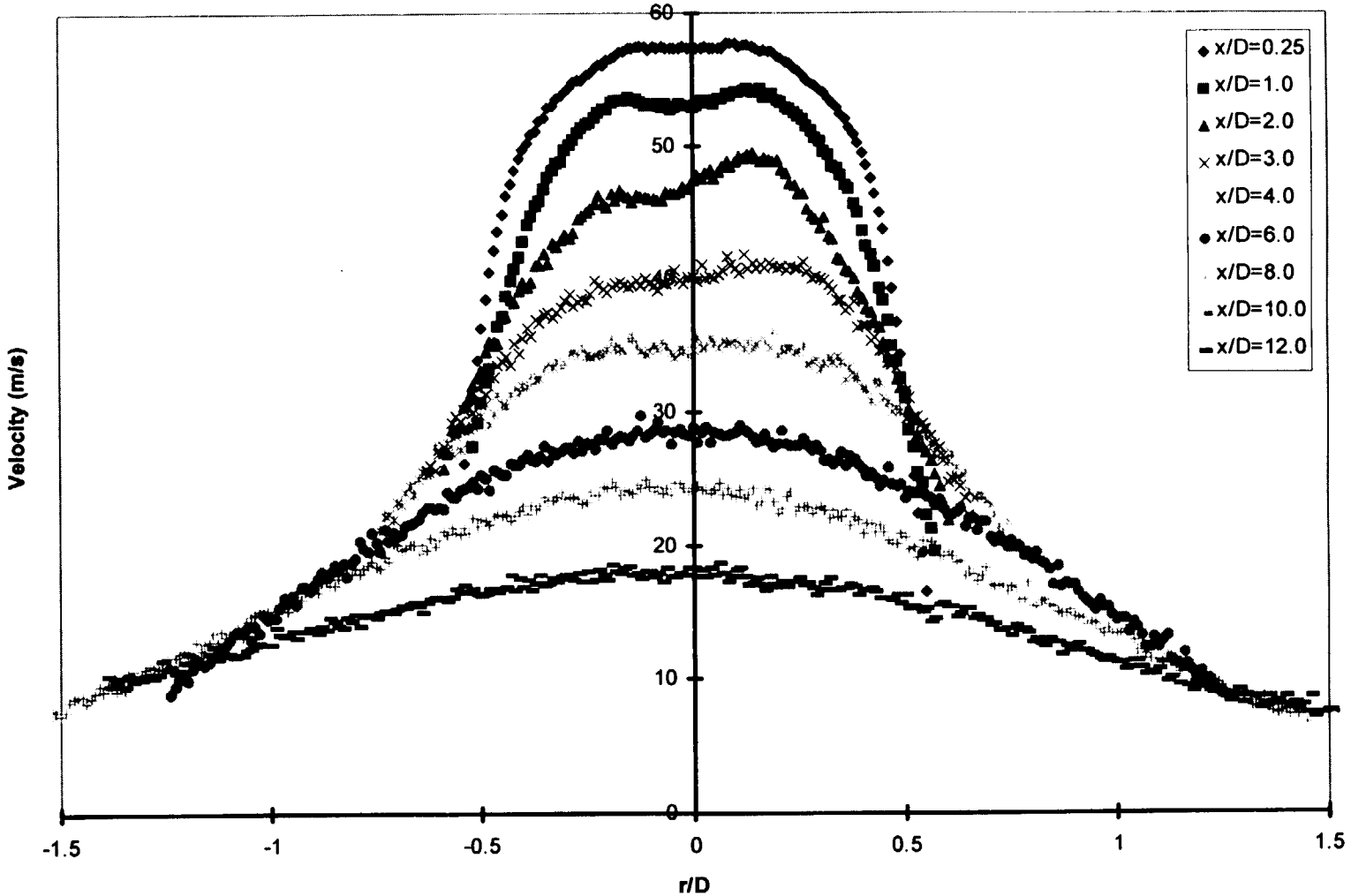

Fig. 32 Composite plot of PDV axial mean velocities for swirling jet; Run 1

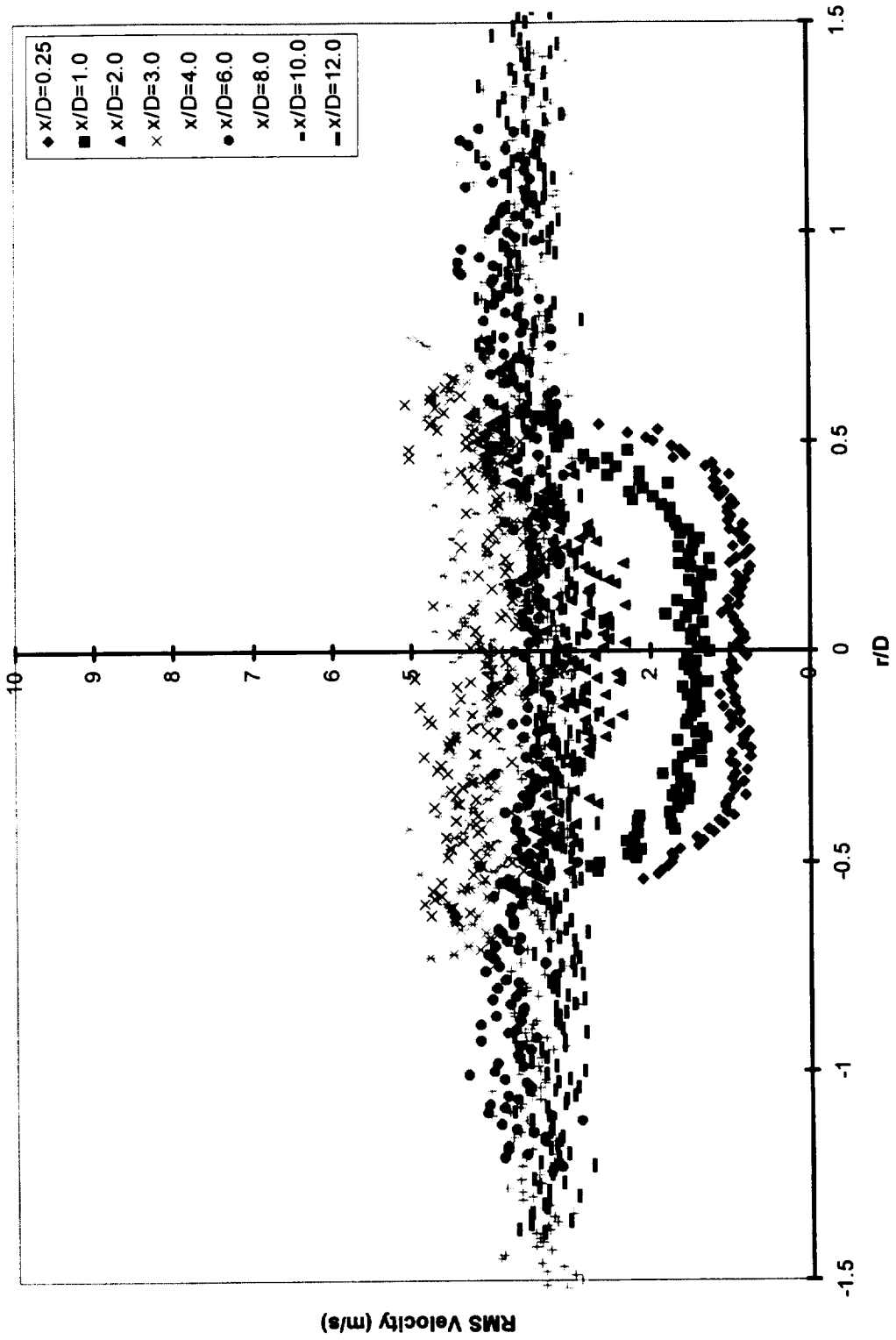

Fig. 33 Composite plot of PDV axial RMS velocities for swirling jet; Run 1

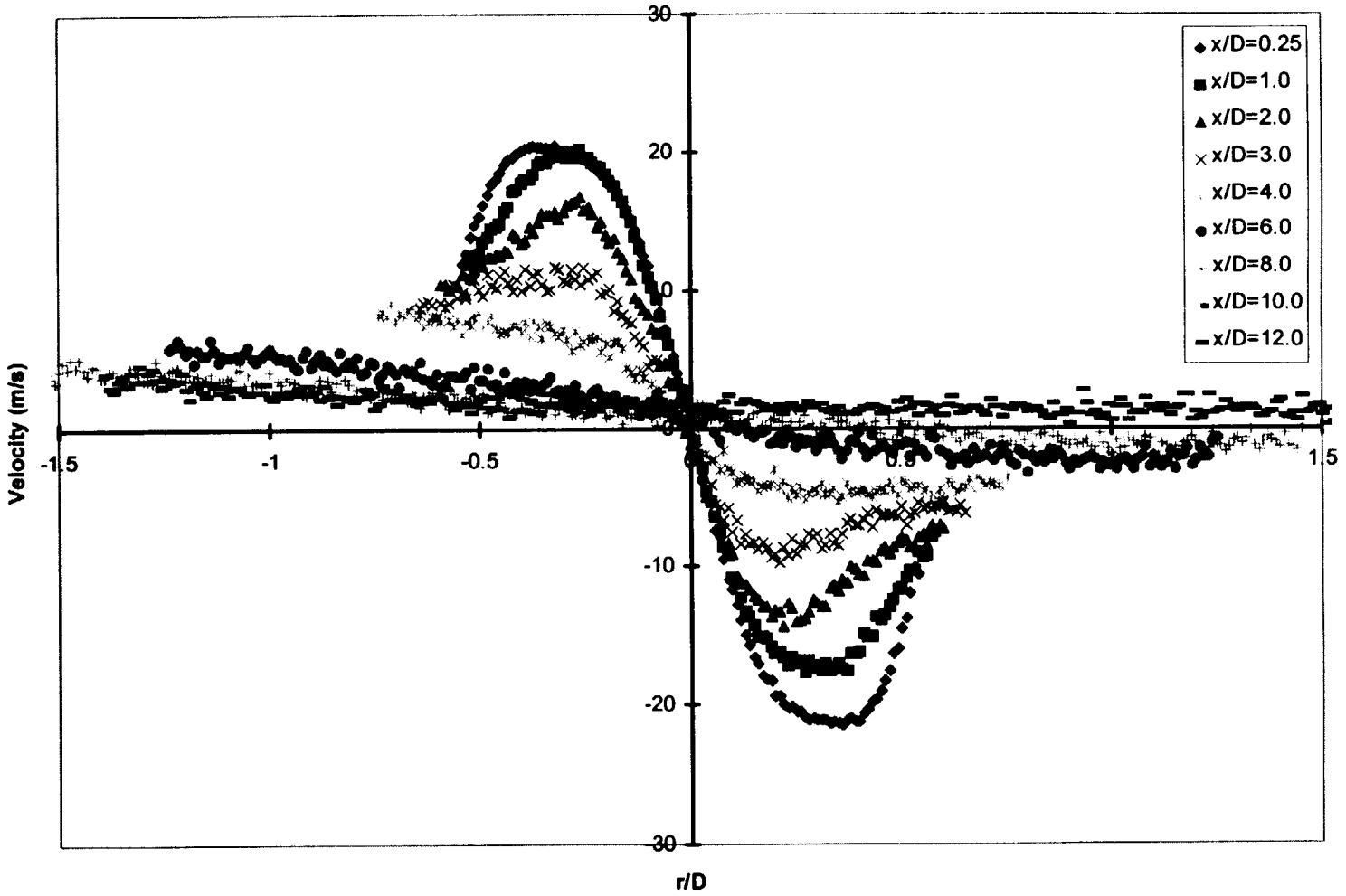

Fig. 34 Composite plot of PDV circumferential mean velocities for swirling jet; Run 1

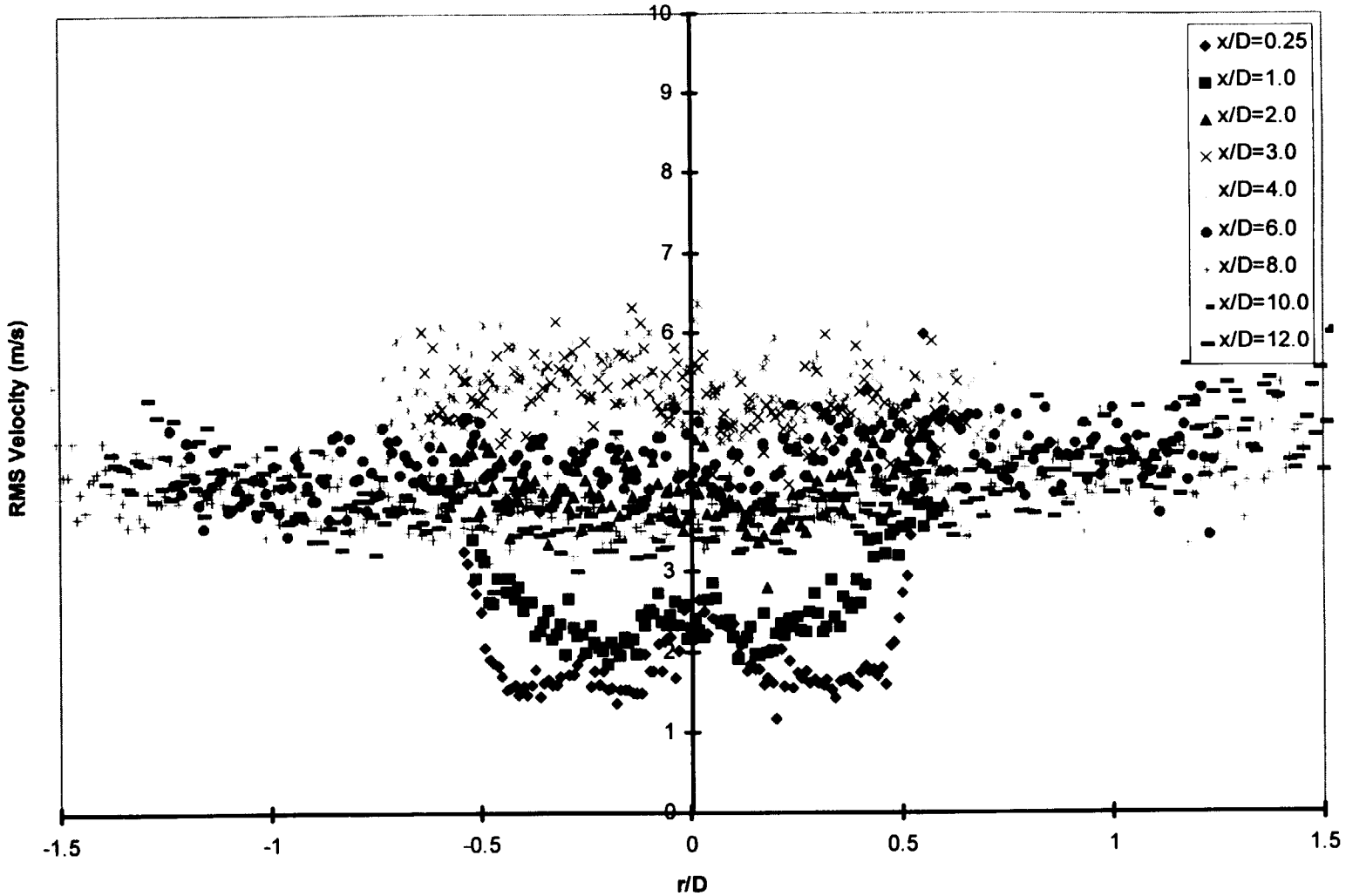

Fig. 35 Composite plot of PDV circumferential RMS velocities for swirling jet; Run 1

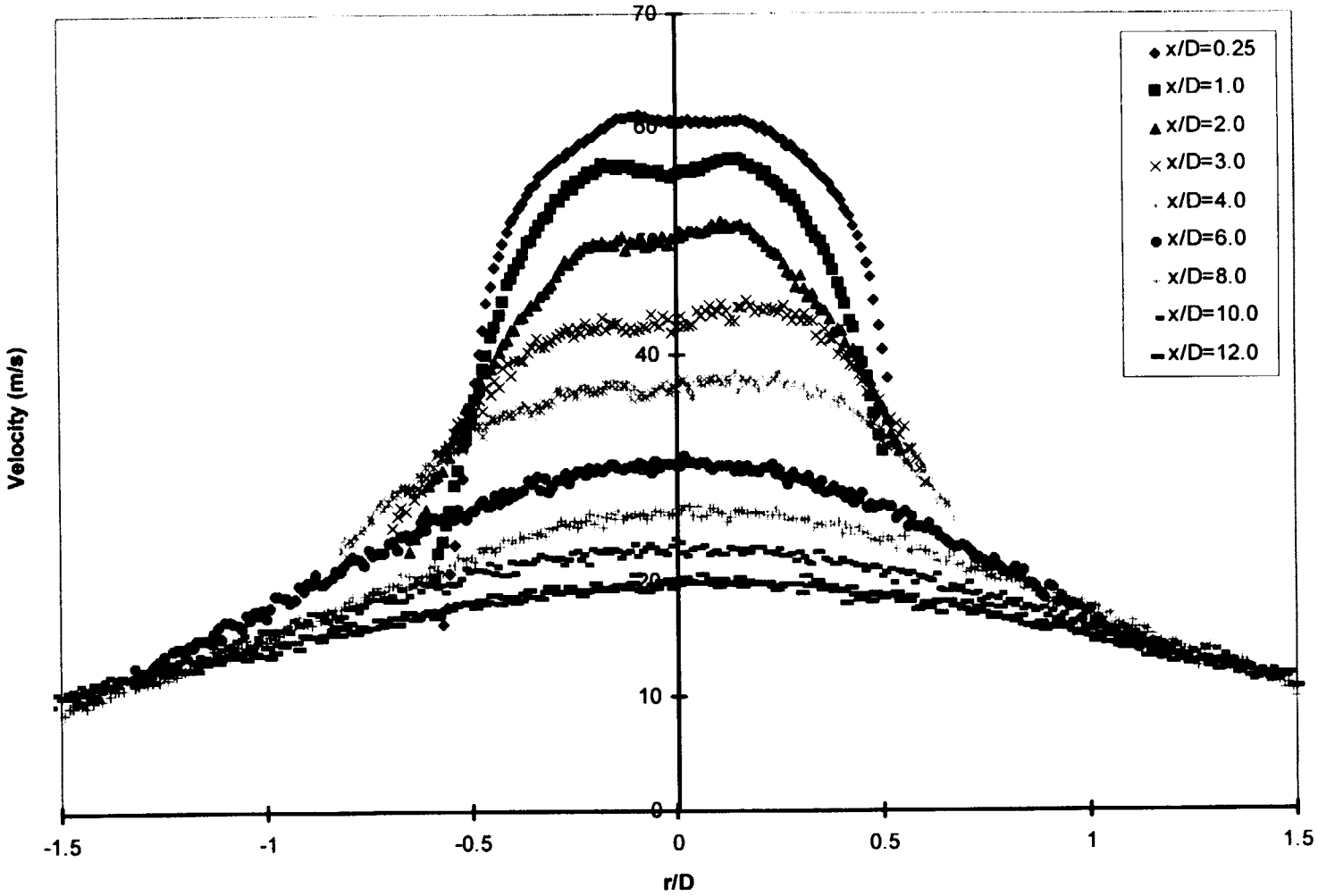

Fig. 36 Composite plot of PDV axial mean velocities for swirling jet; Run 2

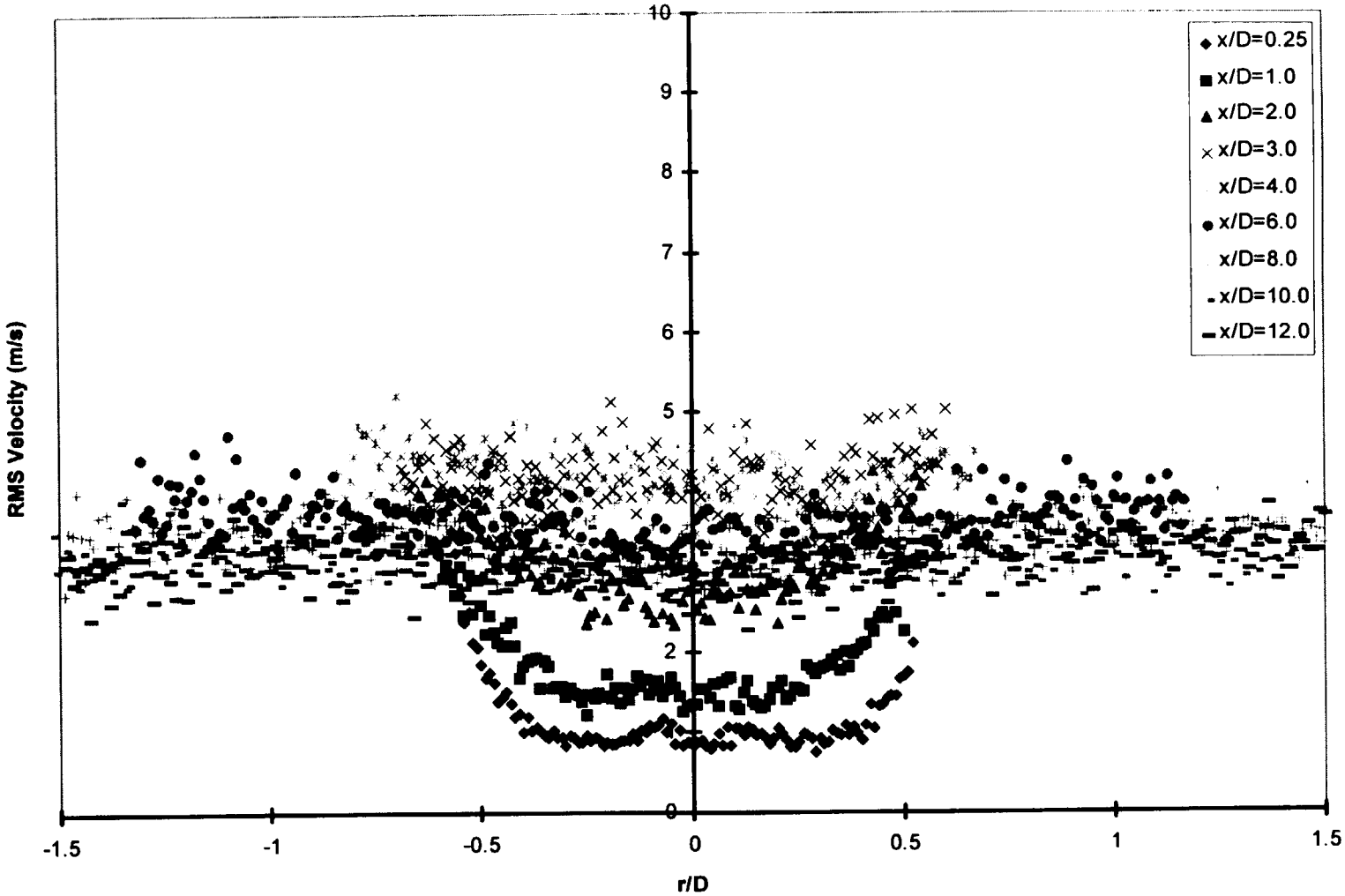

Fig. 37 Composite plot of PDV axial RMS velocities for swirling jet; Run 2

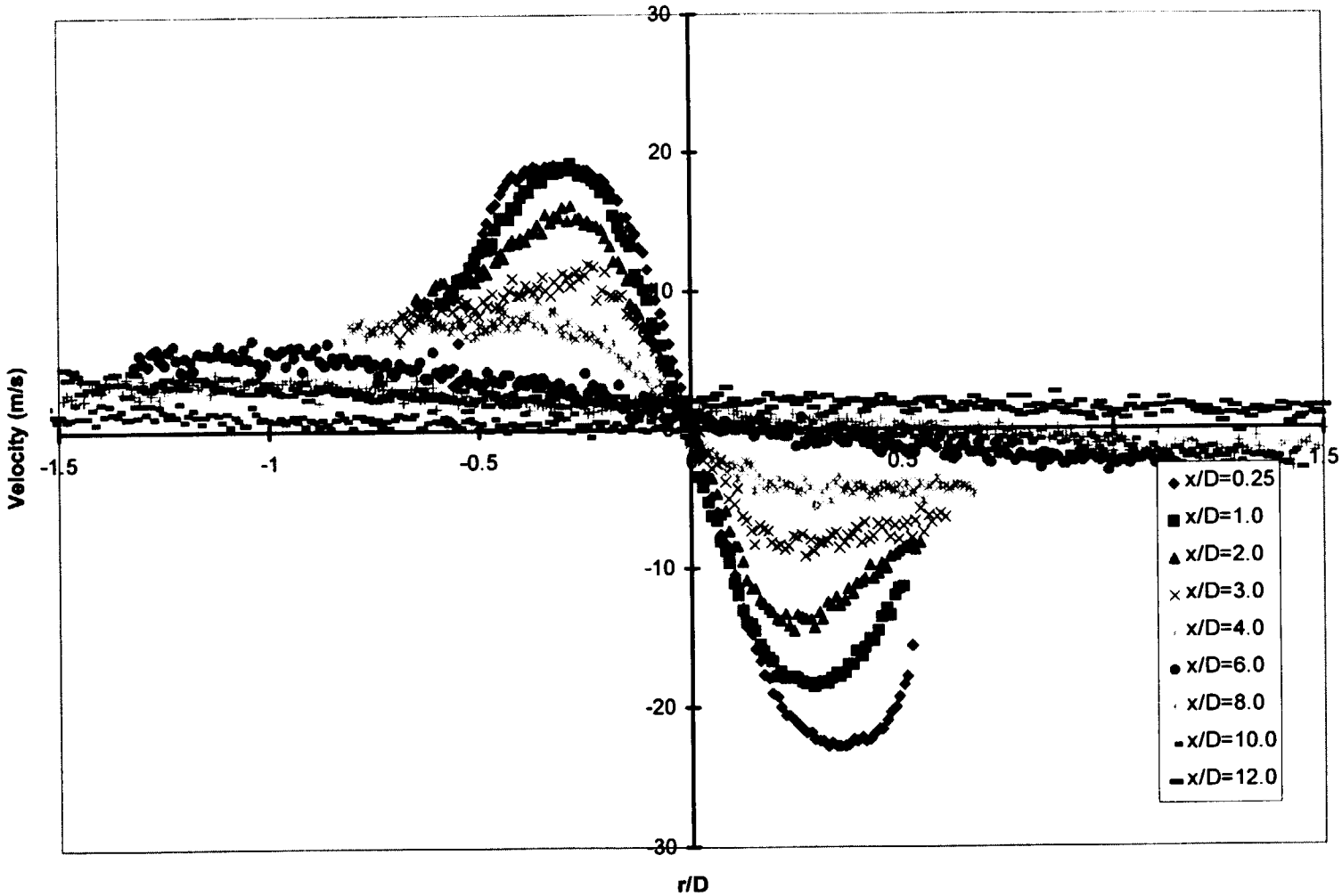

Fig. 38 Composite plot of PDV circumferential mean velocities for swirling jet; Run 2

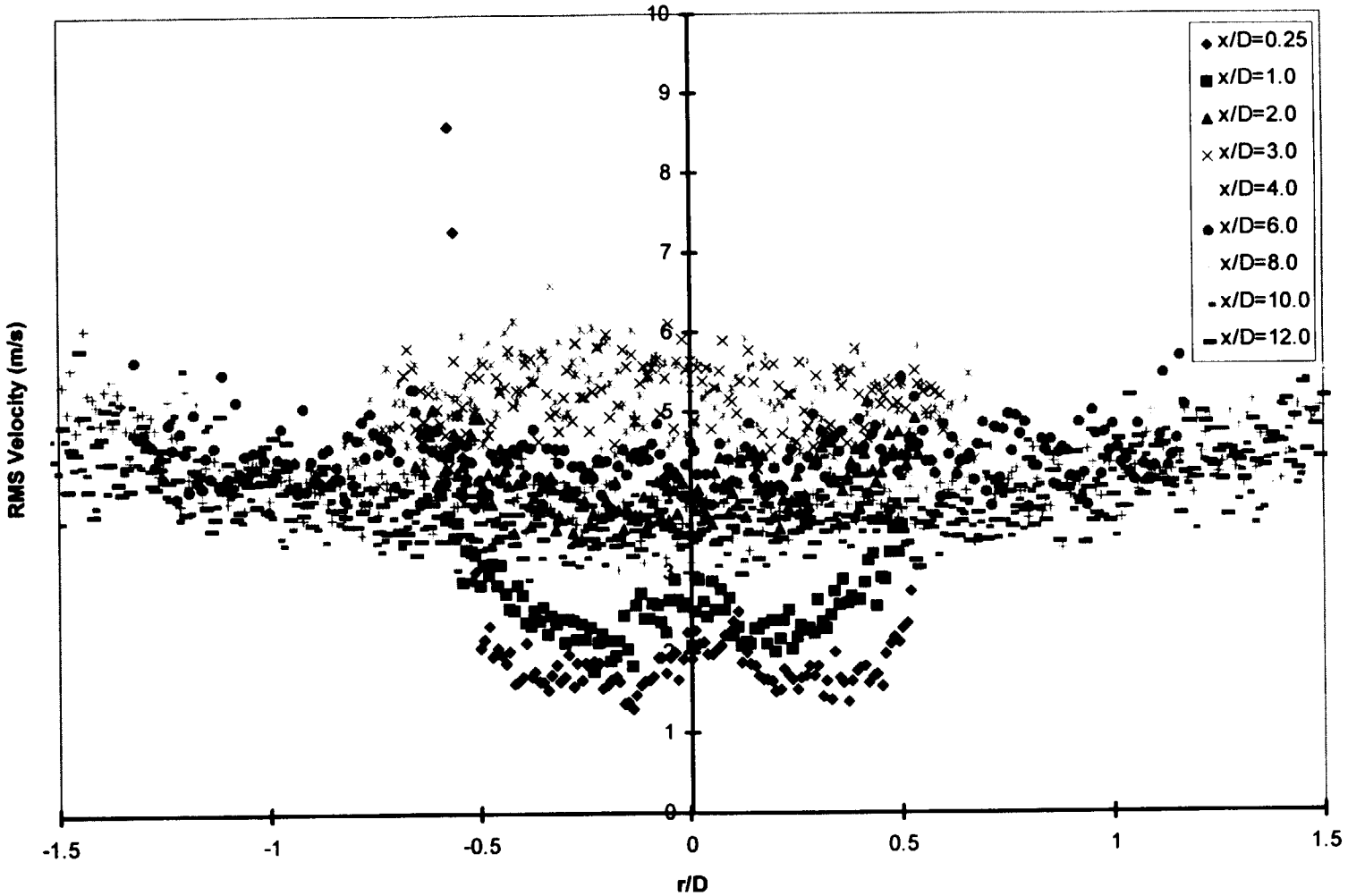

Fig. 39 Composite plot of PDVcircumferential RMS velocities for swirling jet; Run 2

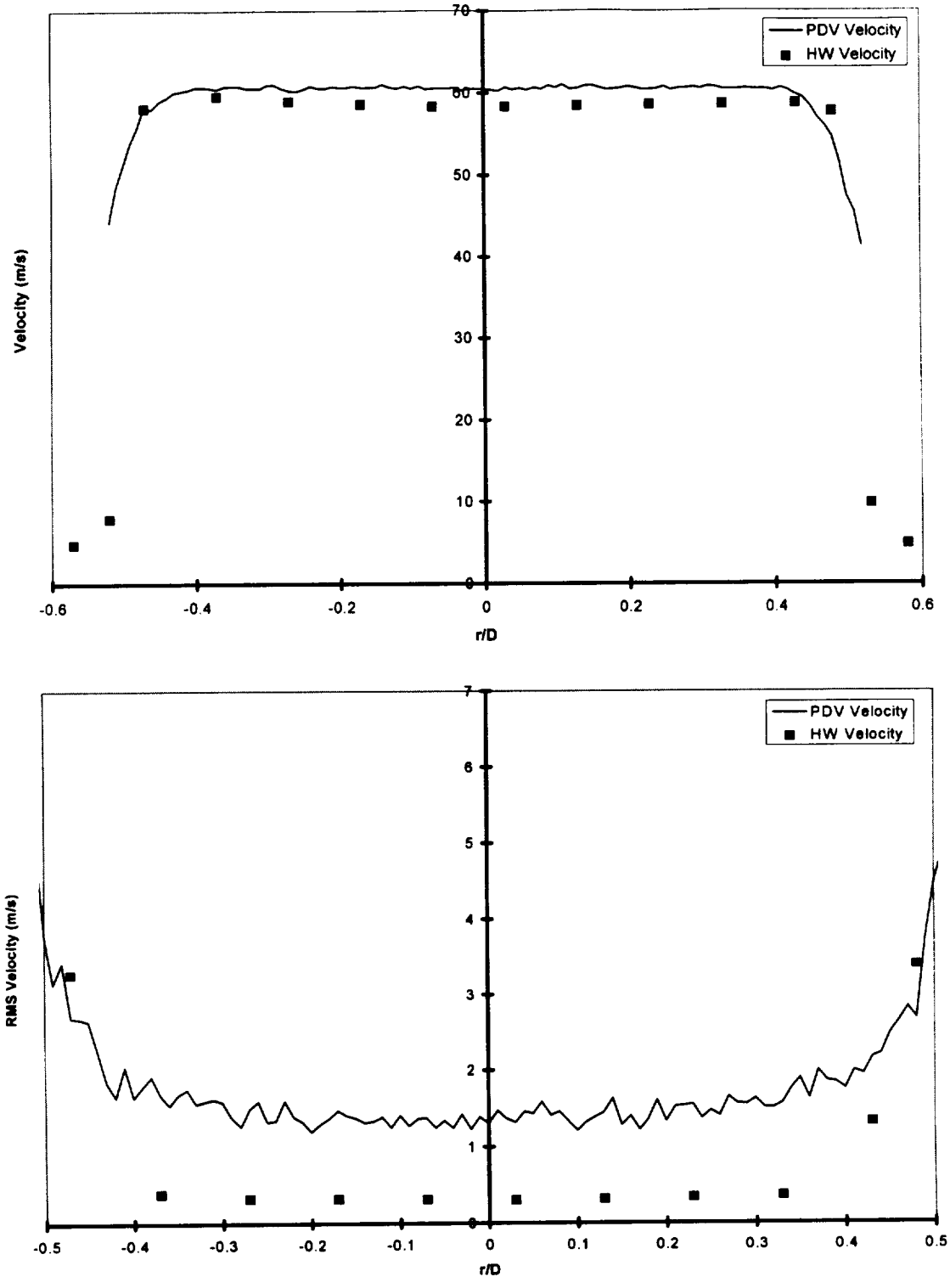

Fig. 40 Comparison plot of PDV Run 2 and hot wire results for standard jet: Exit Profiles
a.) mean axial velocities
b.) RMS axial velocities

10-1-99

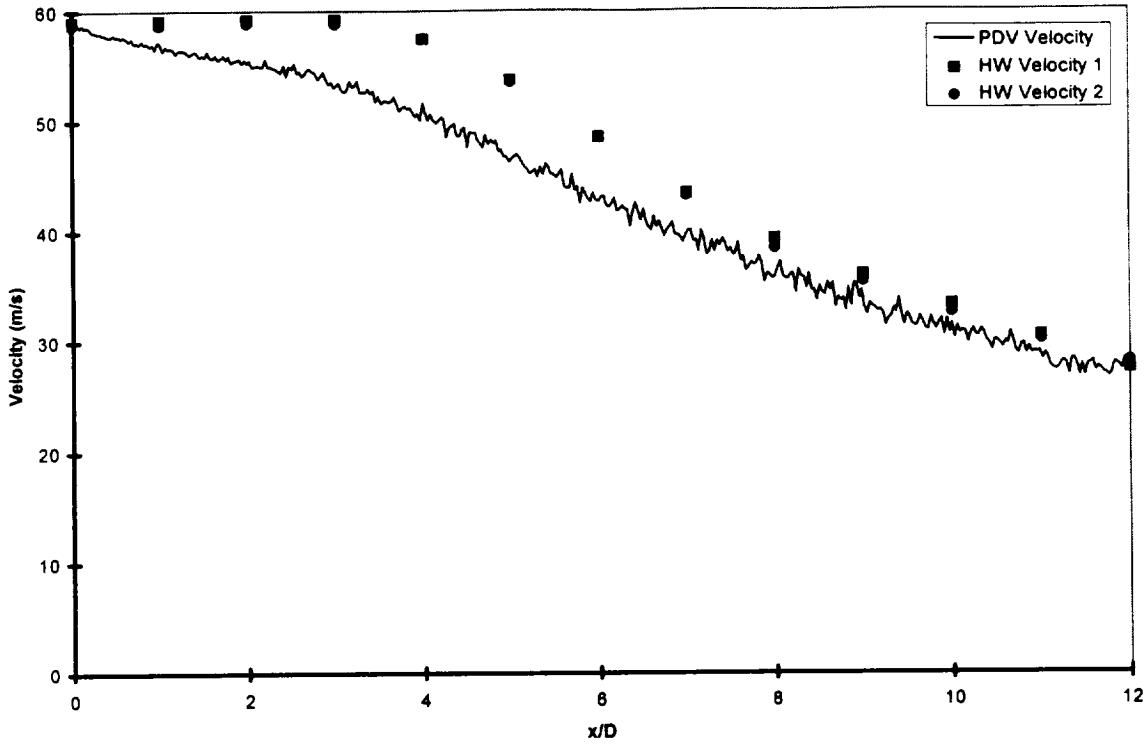

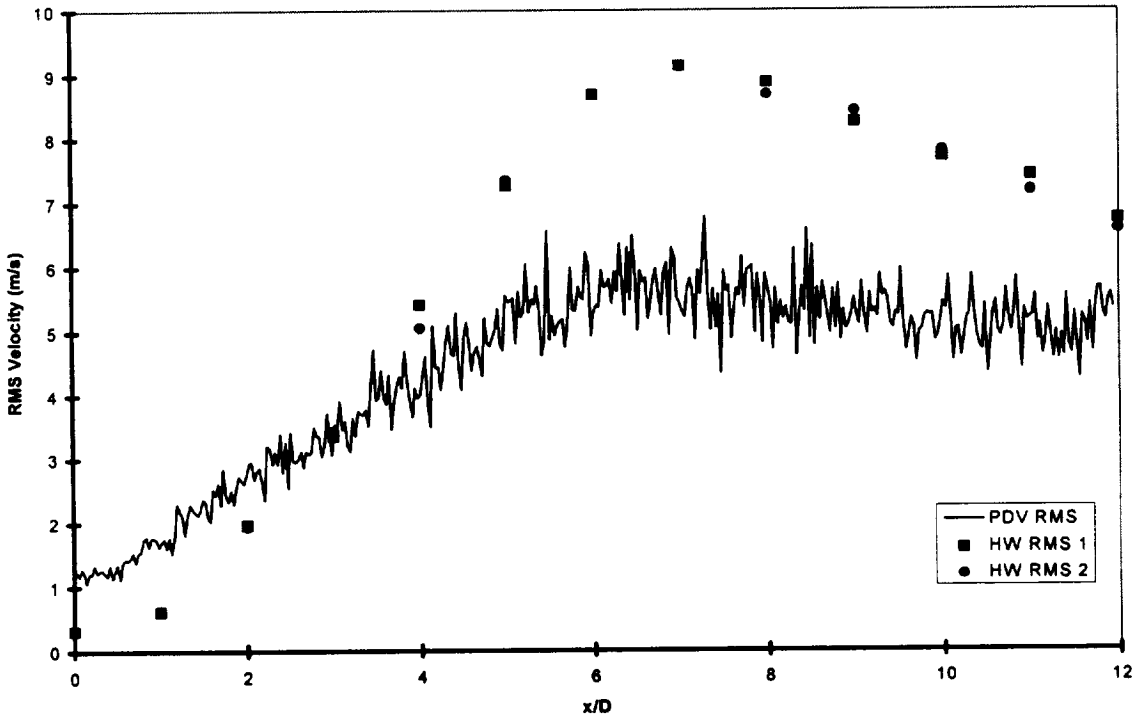

Fig. 41 Comparison plot of PDV Run 2 and hot wire results for standard jet: Centerline
a.) mean axial velocities
b.) RMS axial velocities

10-1-99

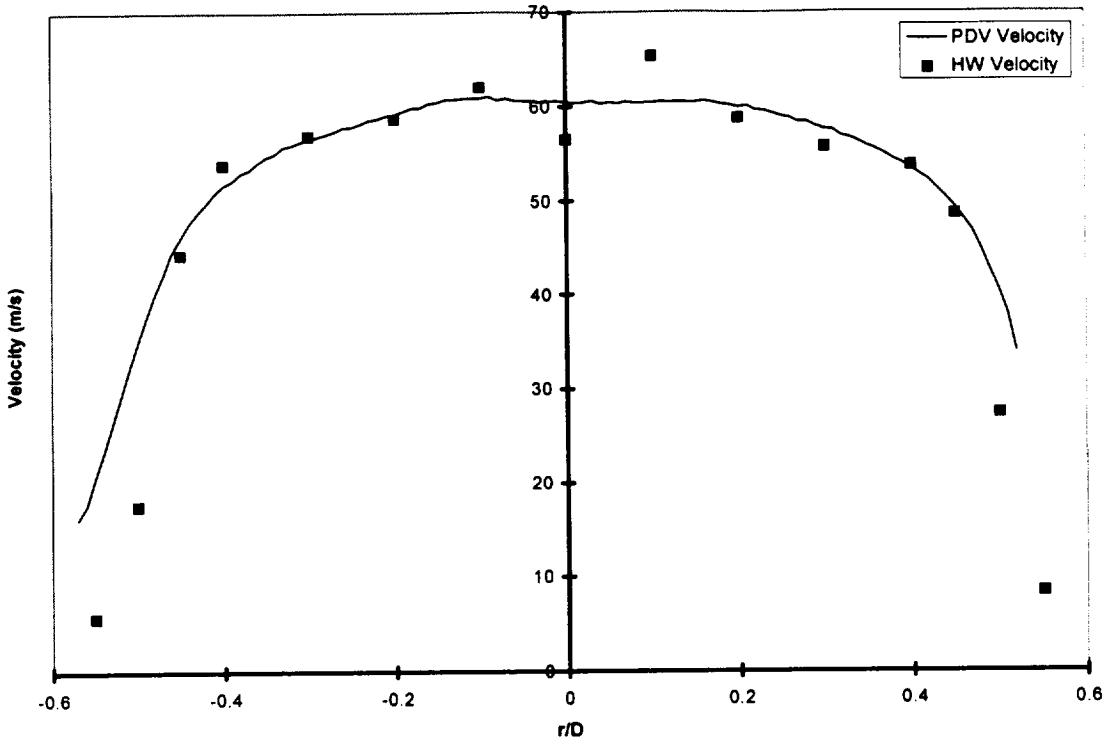

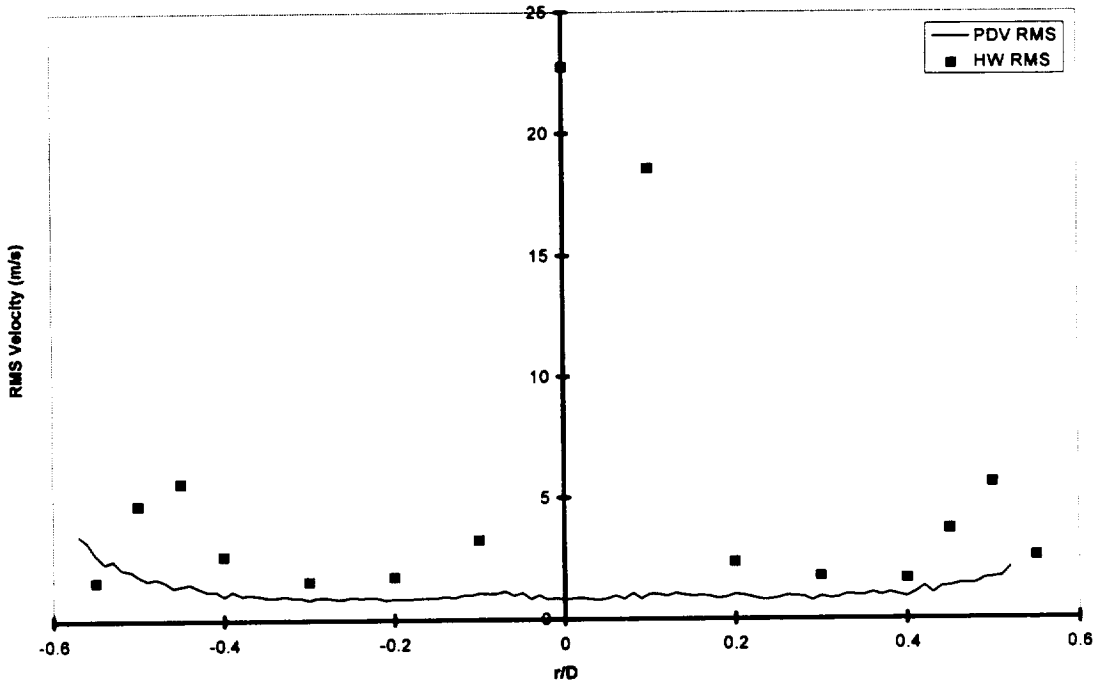

Fig. 42 Comparison plot of PDV Run 2 and hot wire results for swirling jet: Exit Profiles
a.) mean axial velocities
b.) RMS axial velocities

3-14-2000

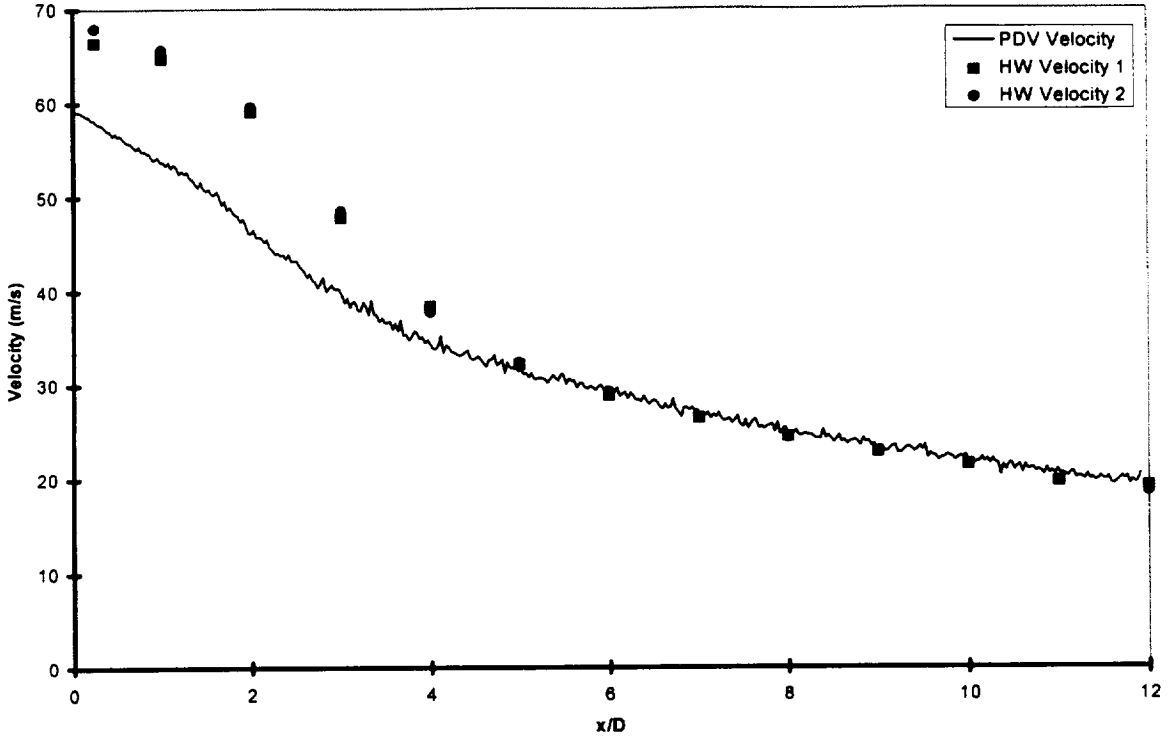

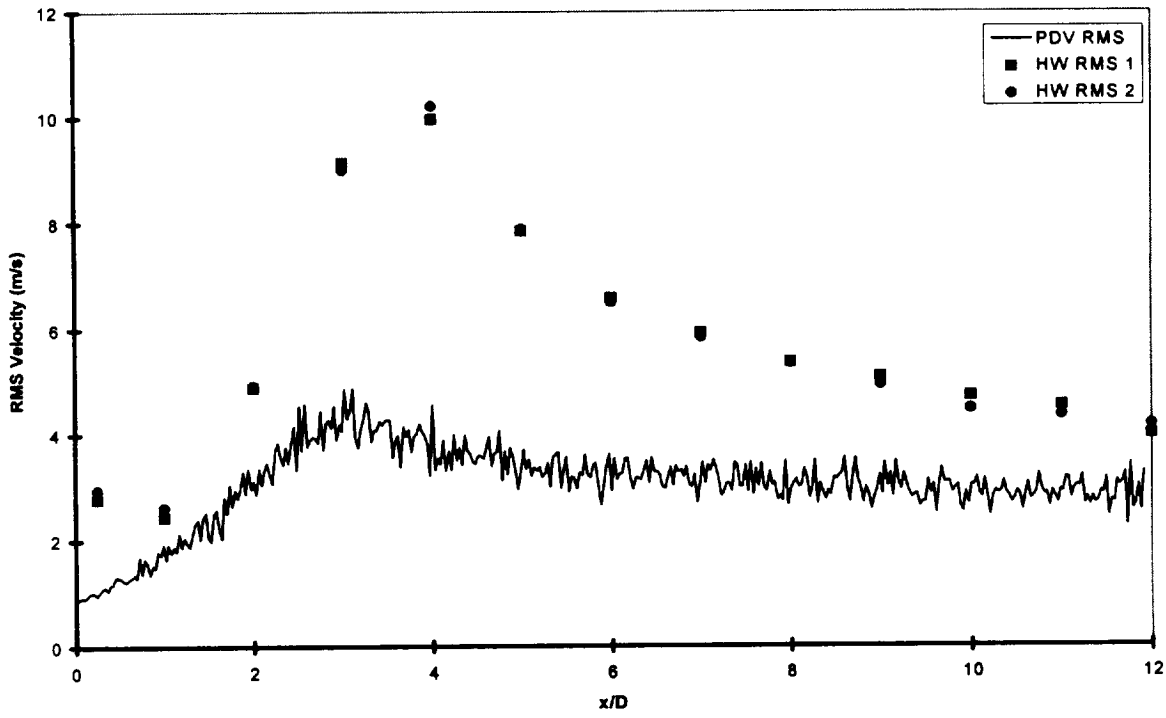

Fig. 43 Comparison plot of PDV Run 2 and hot wire results for swirling jet: Centerline
a.) mean axial velocities
b.) RMS axial velocities

3-14-2000